Disrupted stimulus encoding shapes tactile perception in autism.

Ourania Semelidou[1,2,#], Théo Gauvrit[1,2], Célien Vandromme[1,2,3], Alexandre Cornier[1,2], Anna Saint-Jean[1,2], Yves Le Feuvre[1,2], Melanie Ginger[1,2], Andreas Frick[1,2,#]

[1] INSERM, U1215 Neurocentre Magendie, 33077, Bordeaux, France
[2] University of Bordeaux, 33000, Bordeaux, France
[3] University of Lille, 59000, Lille, France
[#] Co-corresponding authors: ourania.semelidou@inserm.fr, andreas.frick@inserm.fr

Summary

Atypical sensory experience is a core characteristic of autism, significantly affecting daily life. Tactile perception is prominently impacted in autism, including difficulties in the detection and discrimination of low-level stimuli. However, we do not know the neural underpinnings of low-level tactile perception and how they change in autism. Using a translational perceptual task we recapitulate the multifaceted tactile features of autistic individuals in the *Fmr1*$^{-/y}$ mouse model of autism and show tactile hyposensitivity, interindividual variability, and unreliable responses. Using concomitant population activity imaging of pyramidal neurons and GABAergic interneurons, we reveal weak stimulus encoding in the primary somatosensory cortex of *Fmr1*$^{-/y}$-hyposensitive mice. Disrupted encoding renders perception more vulnerable to the ongoing network state and impedes reliable response decoding. Increasing the number and reliability of stimulus-recruited neurons by targeting the large conductance calcium-activated potassium (BK_{Ca}) channels improves tactile perception. Our work shows an evolutionarily conserved role for the primary somatosensory cortex in tactile detection and presents a highly translational approach for probing neuronal-perceptual changes in neurodevelopmental conditions.

Introduction

Tactile perception is crucial to exploring and interacting with the world, with the skin being the largest sensory organ. Two-thirds of autistic individuals present alterations in tactile perception, which together with other sensory features constitute one of the core diagnostic criteria of the condition[1,2]. Tactile alterations strongly impact daily life while also contributing to the development of other core symptoms, including difficulties in social communication and interaction, and repetitive behaviors[3–5]. In concrete terms, such alterations include differences in the detection and discrimination of tactile stimuli (perceptual sensitivity), overall behavioral responsivity, and sensory-related neuronal responses[6].

The tactile features of autism are highly heterogeneous across individuals, a characteristic reflected in the DSM-5 as "hyper- or hypo-reactivity to sensory input"[7–11]. This sensory heterogeneity might be explained by the stimulus characteristics and the stimulated body part. For example, objective measures of perceptual sensitivity showed that the detection of vibrotactile stimuli delivered to the fingers depends on the stimulus frequency, with hyposensitivity to low-level stimulation[12,13] and typical detection of higher-frequency vibrotactile stimuli[14] in autism. Conversely, low-level vibrotactile stimuli delivered to the forearm and

representing the social/affiliative submodality of somatosensation revealed hypersensitivity in autistic individuals[15].

Tactile information is relayed from the periphery to the primary somatosensory cortex, where it is processed and further integrated[16]. In autistic individuals, tactile stimulation revealed diminished[17] or increased[18] early responses, decreased late responses[18], reduced GABA levels[19,20], and different cortical representations of tactile stimuli[21] within the somatosensory cortex. However, these neuronal responses are rarely combined with perceptual measures[19], leaving a knowledge gap regarding the neural correlates of altered tactile perception in autism. Moreover, technical limitations in human studies prevent measurements of neuronal population dynamics at the single-cell resolution required to uncover the neocortical underpinnings of altered tactile perception.

Integrating psychophysics with physiological measurements provides an objective and quantifiable method for examining how tactile-related neuronal responses impact perceptual sensitivity. Such an approach revealed a link between the dysfunction of GABAergic interneurons in the whisker-related primary somatosensory cortex and perceptual hypersensitivity to whisker stimuli in Shank3B$^{-/-}$ mice[22].

Here, we took advantage of the similarity between the somatosensory systems of the forepaw of mice and the human hand[23–25] to develop a highly translational platform for studying the nuanced sensory symptomatology of autism together with neuronal activity during perception. We established a standardized approach for rodent models to assess perceptual sensitivity in autism (Fig. 1a), uncover its neural correlates, and test mechanism-based treatments. We show that the multifaceted and heterogeneous tactile features of autism can be recapitulated in the well-established *Fmr1*$^{-/y}$ mouse model of autism[26]. We found high interindividual variability in tactile perception, revealing a subgroup of *Fmr1*$^{-/y}$ mice with a tactile hyposensitivity phenotype and unreliable responses. We demonstrate a crucial role for the primary somatosensory cortex (S1-FP) in the detection of low-level (low amplitude and frequency) tactile stimuli, showing that sparse stimulus encoding in S1-FP is linked to perception and sufficient to decode behavioral responses. We reveal decreased numbers of activated pyramidal neurons and reduced inhibition during detection in *Fmr1*$^{-/y}$-hyposensitive mice, resulting in weak sensory encoding. Disrupted encoding renders tactile detection more vulnerable to the ongoing network state and impedes reliable response decoding. Strengthening sensory encoding and reducing its variability through activation of the large conductance calcium-activated potassium (BK_{Ca}) channels, recently targeted to ameliorate auditory responsivity[27], improves tactile perception of *Fmr1*$^{-/y}$ mice.

Results

Forepaw-based perceptual decision-making task assesses tactile detection in mice

To study the perception of vibrotactile stimuli, we back-translated a task used in human studies[12,13] and developed a Go/No-Go detection task in head-fixed mice. We combined this task with two-photon calcium imaging to examine the neural correlates of tactile perception within the primary somatosensory neocortex (S1). Water-restricted *Fmr1*$^{-/y}$ mice and their wild type (WT) littermates were trained to associate the delivery of a fixed, suprathreshold vibrotactile stimulus (15 µm, 40 Hz) with a water reward (Go trial; Fig. 1a-left). During Go trials, vibrotactile

stimuli (500 ms) were delivered to the right forepaw of the mice, followed by a 2 s response window during which the mice could lick to trigger water reward delivery (Fig. 1a-left). No-Go (catch) trials in which no stimulus was presented were used to assess spontaneous licking (Fig. 1a-right).

To evaluate sensory perception, we quantified four behavioral outcomes: Hit for successful and Miss for unsuccessful Go trials, and Correct Rejection (CR) for successful and False Alarm (FA) for unsuccessful No-Go trials (Fig. 1a-right). Mice completed the training period when they met our learning criterion, with a performance exceeding an average 70% Hit rate with less than a 30% False Alarm rate for three consecutive training days (Fig. S1a). Pre-stimulus licking (3-8 s before stimulus onset) canceled stimulus delivery and led to a 5 s timeout. 86% of the WT mice and 73% of the *Fmr1*$^{-/y}$ mice reached the learning criterion, with no difference between the learning performances of the two groups (Fig. S1b). Similarly, no genotype effect was observed for the training duration of mice that learned the task (Fig. S1c). These data show that *Fmr1*$^{-/y}$ mice can learn the detection task, with a success rate and training duration similar to their WT littermates.

Fmr1$^{-/y}$ mice show perceptual hyposensitivity for low-level vibrotactile stimuli

Autistic individuals exhibit hyposensitivity to low-level (<25 µm amplitude, 25 Hz frequency) vibrotactile stimulation delivered to the fingers[12,13]. We tested whether we could replicate this phenotype in a preclinical model of autism using similar stimuli in our translational task. We assessed the tactile sensitivity of mice that met the learning criterion during the training period by delivering novel vibrotactile stimuli of low, fixed frequency (10 Hz) at 6 different amplitudes (range: 2-12 µm, 2 µm interval) in a pseudorandom manner. Mice reported the detection of a given stimulus by licking to receive a water reward. By analyzing the Hit rates for all stimulus amplitudes of sessions with low spontaneous licking (<40%), we generated psychometric curves (Fig. 1b) enabling us to determine for each mouse the detection threshold (stimulus amplitude detected in 50% of the trials, curve inflection point), perceptual accuracy (curve slope), and licking strategy (criterion c'; i.e, how liberally or conservatively the mice licked while trying to get the reward).

Fmr1$^{-/y}$ mice exhibited decreased tactile sensitivity (Hit rates) across the entire amplitude range (Fig. 1b), resulting in increased detection thresholds (Fig. 1c) and a trend for lower perceptual accuracy (Fig. S1d) compared to their WT littermates. This difference in detection was not due to alternative strategies adopted by the mice to obtain the reward, as indicated by the similar values of the criterion c' (Fig. S1e). Our results recapitulate the findings in autistic individuals, with *Fmr1*$^{-/y}$ mice showing perceptual hyposensitivity to low-level vibrotactile forepaw stimulation.

Fmr1$^{-/y}$ mice show increased interindividual variability during tactile detection

High interindividual variability in behavior and sensory stimulus-evoked neural responses has become recognized as a hallmark of autism over the last 15 years[18,28–31]. However, this feature of autism has not been recapitulated in mouse models of the condition. We examined whether differences in interindividual variability can also be observed in our mouse model by comparing the group variance of the Hit rates for each amplitude during tactile detection. Our results demonstrate higher interindividual variability in the *Fmr1*$^{-/y}$ group compared to WT mice, with a

statistically significant increase in variance observed for all stimuli exceeding the amplitude of 4 µm (Fig. 1d).

Further inspection of the responses of *Fmr1*$^{-/y}$ mice suggested the existence of discrete subgroups. We therefore used K-means clustering on the Hit rates across amplitudes to divide the *Fmr1*$^{-/y}$ cohort into two subgroups. Consistent with findings from autistic individuals that revealed subgroups based on sensory difficulties[29], one subgroup of *Fmr1*$^{-/y}$ mice exhibited tactile stimulus detection comparable to that of WT mice, while the second subgroup displayed strongly diminished tactile sensitivity across all stimulus amplitudes (here referred to as *Fmr1*$^{-/y}$-hyposensitive mice; Fig. 1e). This reduced sensitivity of *Fmr1*$^{-/y}$-hyposensitive mice is evidenced by an elevated perceptual detection threshold (Fig. 1f) and decreased perceptual accuracy (cf. *Fmr1*$^{-y}$ and WT group) (Fig. 1g). Importantly, no genotype differences were observed in strategy (Fig. 1h) and learning abilities (Fig. 1i, Fig. S1f).

Intrigued by the perceptual differences within the *Fmr1*$^{-/y}$ cohort, we explored possible causes for this phenotypic heterogeneity. We first verified that mice of both subgroups came from the same litters, and controlled for the age of the parents and the experience of the mother, thus excluding the possibility of litter- or breeder-specific variability[32]. We also verified that there was no difference in the size of the litters between the two groups, which positively correlates with behavioral alterations in mice[33] (Fig. S1g). Finally, we measured the body weight, which inversely correlates with sensitivity to visual stimuli in vertebrates[34], as does the metabolic rate in humans[35]. *Fmr1*$^{-/y}$-hyposensitive mice weighed on average 2.5 g more than the WT animals before water restriction, a difference that was not observed between WT mice and the other *Fmr1*$^{-/y}$ subgroup (Fig. S1h). Noteworthy, metabolic alterations have previously been described in the context of autism[36–40].

These results demonstrate an increased inter-individual variability within the *Fmr1*$^{-/y}$ cohort, with tactile hyposensitivity in one subgroup of *Fmr1*$^{-/y}$ mice that also exhibits increased body weight.

Increased intra-individual variability across stimulus trials in *Fmr1*$^{-/y}$-hyposensitive mice

Increased intra-individual variability has been observed in the behavioral and neuronal responses of autistic individuals[8,41–45]. However, in preclinical models of autism, intra-individual variability in sensory perception has not yet been described. Our results of reduced perceptual accuracy among the *Fmr1*$^{-/y}$-hyposensitive mice (Fig. 1g) suggest that sensory perception in these animals is less reliable. To further investigate this idea, we assessed the trial-by-trial (TBT) variability in the behavioral response for each stimulus amplitude in Go trials (Hit vs Miss). As expected, response variability increased close to threshold stimulation for both WT mice and *Fmr1*$^{-/y}$ mice with intact perception (Fig. 1j). Conversely, *Fmr1*$^{-/y}$-hyposensitive mice exhibited increased TBT variability for all stimulus amplitudes above 6 µm, and increased mean variance of responses across all amplitudes compared to the other groups (Fig. 1j).

We further examined genotype differences in response variability specifically for threshold and non-threshold stimuli. We compared the TBT variability of responses at the threshold amplitude (50% Hit rate), as well as the first sub-threshold and supra-threshold amplitude for each mouse. As expected, all groups showed a large TBT variability for responses to the threshold amplitude.

However, *Fmr1*$^{-/y}$-hyposensitive mice exhibited highly variable responses also for sub- and suprathreshold stimulus amplitudes (Fig. 1k). These data show unreliable responses in *Fmr1*$^{-/y}$-hyposensitive mice across the range from sub- to supra-threshold stimuli and reproduce one of the hallmark characteristics reported for autistic individuals.

Fmr1$^{-/y}$ mice present behavioral hypo-responsivity in response to tactile stimulation

There is a growing appreciation of the heterogeneous nature of sensory features that include not only differences in perceptual sensitivity but also in the behavioral responsivity to sensory stimuli[6]. We probed alterations in tactile responsivity in *Fmr1*$^{-/y}$ mice by employing an adhesive removal task[46], in which we attached an adhesive tape to each forepaw of the mice and measured the time they took to make their first contact with the tape. This delay assesses the behavioral responsivity of mice to a prolonged, non-aversive, non-sinusoidal stimulation. *Fmr1*$^{-/y}$ mice showed hypo-responsivity, with a longer delay to their first contact with the adhesive tape (Fig. 1l-left). In contrast, no motor deficits were identified since both groups required the same time to remove the adhesive tape after the first contact (Fig. 1l-right).

Stimulus intensity encoding in S1-FP

To better understand the neural correlates of low-level vibrotactile perception in general, and their potential changes in autism, we recorded responses of populations of excitatory pyramidal neurons and inhibitory GABAergic interneurons at single-cell resolution in the forepaw-related primary somatosensory cortex (S1-FP) of mice during tactile detection (Fig. 2a). The total number of recorded pyramidal neurons and inhibitory interneurons in the field of view was in the range of 50-150 (~20% interneurons, no genotype difference, Fig. S2a-b). Neuronal activity was aligned with tactile stimulation and behavioral response (licking or absence thereof), enabling us to explore the neural dynamics underlying stimuli of different amplitudes, and linking them to sensory detection (Fig. 2b).

According to psychophysics and signal detection theory, stimulus perception emerges from two functions, one describing the transformation of the stimulus and another relating to that of the response[47,48]. In our task, the stimulus transformation function (stimulus encoding) translates the physical characteristics of the stimulus (amplitude and frequency) into a perceptual magnitude. The response transformation function (response decoding) calculates the difference between the perceptual magnitude and noise levels to generate a behavioral response, with a high signal-to-noise ratio resulting in stimulus detection. To assess how each stimulus amplitude is encoded in S1-FP, we calculated the percentage of activated and inhibited neurons during stimulation. We found an increased number of activated pyramidal neurons and GABAergic interneurons as the stimulus amplitude increased, across all groups (Fig. 2c). For inhibition, we found that the number of inhibited pyramidal neurons did not increase with higher stimulus amplitudes, while more GABAergic interneurons were inhibited as the stimulus amplitude increased (Fig. 2d).

Given that stimuli with higher amplitude are more easily detected, the ratio of detected to non-detected trials increased with amplitude. To determine if the neural responses encode for the stimulus amplitude independently of its detection, we compared the number of recruited (activated or inhibited) neurons during detected trials for each amplitude. Our results show an

effect for stimulus amplitude in the number of activated pyramidal neurons (Fig. 2e-top) but not in that of activated GABAergic interneurons (Fig. 2e-bottom), inhibited pyramidal neurons (Fig. S2c-top), or inhibited GABAergic interneurons (Fig. S2c-bottom).

Taken together, these results show that low-level vibrotactile stimulus amplitude is encoded in S1-FP primarily by the number of activated pyramidal neurons.

Weak perceptual magnitude in *Fmr1*$^{-/y}$-hyposensitive mice

How are low-level vibrotactile stimuli encoded within S1-FP of *Fmr1*$^{-/y}$ mice? *Fmr1*$^{-/y}$ mice with intact tactile detection (thresholds and accuracy similar to WT mice) did not present any alterations in the number of recruited neurons compared to their WT littermates (Fig. 2c-e). In contrast, neuronal recruitment was significantly decreased in *Fmr1*$^{-/y}$-hyposensitive mice. Both pyramidal neurons and GABAergic interneurons were activated at significantly reduced numbers for most stimulus amplitudes in these mice, reaching WT levels only for the strongest stimulus (12 µm amplitude) (Fig. 2c). Conversely, levels of inhibited neurons (pyramidal neurons and GABAergic interneurons) were similar between all three groups (Fig. 2d). Similarly, there was no difference in the number of activated neurons during detected trials across all three groups (Fig. 2e).

These results show that *Fmr1*$^{-/y}$-hyposensitive mice show significantly decreased neuronal activation during stimulation, resulting in weaker perceptual magnitude that correlates with their perceptual hyposensitivity (Fig. 1f-g). In contrast, no differences were observed in the neuronal responses of the *Fmr1*$^{-/y}$ mice with typical tactile detection, explaining their intact perceptual performance.

Perceptual magnitude during detection depends on neuronal inhibition in WT but not in *Fmr1*$^{-/y}$-hyposensitive mice

To determine which specific features of stimulus encoding enable effective sensory detection and might explain poor performance in *Fmr1*$^{-/y}$-hyposensitive mice, we compared the number of recruited neurons between detected (Hit) and non-detected (Miss) trials regardless of stimulation intensity. We found five times more activated pyramidal neurons during detected trials (cf. non-detected trials) in WT mice vs three times more in *Fmr1*$^{-/y}$-hyposensitive mice (Fig. 2f-top). In WT mice, this increased activation of pyramidal neurons during detection was accompanied by an increased number of inhibited pyramidal neurons and GABAergic interneurons (Fig. 2g). This was not the case for *Fmr1*$^{-/y}$-hyposensitive mice, which showed only a trend for an increase in the number of inhibited pyramidal neurons (Fig. 2g-top) and no change in the number of inhibited GABAergic interneurons (Fig. 2g-bottom). Interestingly, *Fmr1*$^{-/y}$-hyposensitive mice presented fewer activated GABAergic interneurons during non-detected trials compared to detected ones (Fig. 2f-bottom), indicating decreased sensory gating due to reduced feedforward inhibition[19].

To ensure that the neuronal responses were stimulus-specific and not affected by licking or movement, we compared the percentage of recruited neurons during the No-Go (catch) trials between *Fmr1*$^{-/y}$-hyposensitive and their WT littermates. We found that the recruitment of pyramidal neurons and GABAergic interneurons in No-Go trials was comparable between the two groups (Fig. S2d) and independent of the behavioral outcome (FA or CR) (Fig. S2e-f).

Based on the results of neuronal recruitment during stimulation, we examined the strength of the perceptual magnitude during detection by calculating the difference in the number of recruited neurons between detected and non-detected trials. Comparison between genotypes showed a trend of less stimulus-recruited pyramidal neurons in *Fmr1*$^{-/y}$-hyposensitive mice (Fig. S2g), demonstrating less differentiated pyramidal responses between detected and non-detected trials in these mice.

These results show a stronger perceptual magnitude in S1-FP for detected stimuli compared to non-detected ones in both groups. In WT mice, the perceptual magnitude in detected trials is encoded by an increased number of activated pyramidal neurons as well as inhibited pyramidal and GABAergic interneurons. In contrast, *Fmr1*$^{-/y}$-hyposensitive mice exhibited decreased stimulus-related inhibition during detection and reduced sensory gating, as well as a weaker perceptual magnitude of detected stimuli.

Stronger and faster responses contribute to the perceptual magnitude during detection in WT but not in *Fmr1*$^{-/y}$-hyposensitive mice

In addition to the number of recruited neurons, the amplitude and the time course of the neuronal responses might also affect the perceptual magnitude created during stimulus encoding (Fig. 2h). To investigate possible differences in the amplitude of neuronal responses between detected and non-detected trials, we calculated the peak amplitude of recruited neurons during stimulation. We found a slight but significant increase in the response amplitude of activated pyramidal neurons and a trend for inhibited GABAergic interneurons during detection in WT mice. This increase was not observed in the *Fmr1*$^{-/y}$-hyposensitive group (Fig. 2i-j).

To examine whether neuronal responses had a different response delay for detected trials we measured the latency of the peak amplitude from the stimulus onset. Our results show faster responses in recruited pyramidal neurons during detected trials in WT mice, but not in *Fmr1*$^{-/y}$-hyposensitive mice (Fig. 2k-l). These data demonstrate a higher response amplitude and faster responses during detected trials contributing to the perceptual magnitude in WT but not *Fmr1*$^{-/y}$-hyposensitive mice.

Perceptual magnitude determines response decoding of threshold stimuli in WT but not in *Fmr1*$^{-/y}$-hyposensitive mice

Our results show that detected stimuli of all amplitudes recruit more neurons in S1-FP compared to non-detected stimuli. Which feature of the perceptual magnitude distinguishes sensory detection from a Miss? To assess this, we looked specifically into threshold stimuli, where the same stimulus amplitude is detected in ~50% of the trials. For these threshold stimuli, WT mice showed five times more activated neurons when the stimulus was detected compared to a Miss (Fig. 3a). Conversely, the number of inhibited neurons, the response amplitude, and the response delay were not different between detected and non-detected threshold trials (Fig. 3b, S3a-b), indicating that perceptual magnitude for threshold stimuli is primarily encoded by the number of activated neurons and not their amplitude or time course.

In contrast, *Fmr1*$^{-/y}$-hyposensitive mice showed only a trend for more activated neurons during detected threshold stimuli compared to non-detected ones (Fig. 3a). This is due to significantly

lower recruitment of pyramidal neurons during detection compared to WT mice (Fig. 3c). Similarly, the difference in the recruited pyramidal neurons between detected threshold trials and No-Go trials was decreased in *Fmr1*$^{-/y}$-hyposensitive mice compared to their WT littermates (Fig. S3c-Detected), showing a decreased signal-to-noise ratio in these mice.

Taken together, our results show that the number of activated pyramidal neurons generates the perceptual magnitude during threshold stimulation, which in turn determines response decoding in WT mice. In contrast, the weak perceptual magnitude in *Fmr1*$^{-/y}$-hyposensitive mice results to decreased signal-to-noise ratio and has less impact on response decoding.

Response decoding in *Fmr1*$^{-/y}$-hyposensitive mice is contingent upon the ongoing network state

In the framework of response transformation, weak perceptual magnitude (Fig. 2c-d, Fig. 3a-c) suggests a strong impact of noise on response decoding in *Fmr1*$^{-/y}$-hyposensitive mice. Increased endogenous neural noise has been suggested to contribute to an enhanced variability of the neuronal responses of the primary somatosensory cortex in anesthetized *Fmr1*$^{-/y}$ mice[49]. However, we do not know the perceptual outcome of this neuronal variability. We computed the average z-score response of each neuron during each threshold stimulus trial and calculated the response TBT variability by measuring the similarity (cosine similarity) between each pair of threshold trials for each mouse. Our results showed higher TBT variability in neuronal responses during detected threshold stimuli in *Fmr1*$^{-/y}$-hyposensitive mice compared to WT (Fig. 3d), indicating that the ongoing network state is impacting stimulus detection.

Increased TBT variability could be the result of different neurons being recruited from trial to trial. To investigate this, we identified all pyramidal neurons recruited by threshold stimuli for each trial and calculated the cosine similarity reflecting the fraction of trials recruiting the same neurons. Our results demonstrate that ~40% of detected trials recruit the same pyramidal neurons in both WT and *Fmr1*$^{-/y}$-hyposensitive mice (Fig. 3e).

We then examined if the increased TBT variability preferentially resulted from the responses of so-called reliable responders — neurons that were recruited in >5 detected stimulus trials. Our analysis revealed that *Fmr1*$^{-/y}$-hyposensitive mice exhibit elevated TBT variability in the activity of both reliable and non-reliable responders (Fig. 3f-g) and have fewer reliable responders compared to their WT littermates (Fig. 3h).

Finally, we investigated the impact of the pre-stimulus activity of pyramidal neurons on stimulus-related responses[49,50] by probing the correlation of TBT variability in the pre-stimulus activity (average activity during 500 ms before stimulus onset) with that during threshold stimulation. Our results demonstrate that the pre-stimulus TBT variability positively correlates with stimulus TBT variability in WT but not in *Fmr1*$^{-/y}$-hyposensitive mice (Fig. 3i). Thus, stimulus encoding is variable in *Fmr1*$^{-/y}$-hyposensitive mice independently of the baseline variability just before the onset of stimulation.

Collectively, these data demonstrate increased TBT variability in neuronal responses during detected threshold stimuli in *Fmr1*$^{-/y}$-hyposensitive mice, indicating a strong impact of the ongoing network state during stimulation onto response decoding. In contrast, strong and reliable

perceptual magnitude in WT mice makes response decoding less vulnerable to the influence of noise within the network.

$Fmr1^{-/y}$-hyposensitive mice show increased excitation-to-inhibition ratio in non-detected trials

Our results show that the detection-related neuronal inhibition in S1-FP is reduced in $Fmr1^{-/y}$-hyposensitive mice (Fig. 2g), possibly contributing to a shift in the excitation-to-inhibition (E/I) balance, a feature of noisy information processing in autism[51]. We examined this hypothesis by dividing the number of activated pyramidal neurons by the number of activated GABAergic interneurons for each trial type. While we did not observe general E/I ratio alterations in $Fmr1^{-/y}$-hyposensitive mice during detected trials (Fig. 3j-left) and No-Go trials (Fig. S3d), non-detected trials were characterized by an increased E/I ratio in these mice compared to their WT littermates (Fig. 3j-right). These results, combined with fewer activated GABAergic interneurons during non-detected trials in $Fmr1^{-/y}$-hyposensitive mice (Fig. 2f), indicate decreased inhibition during non-detected stimuli in $Fmr1^{-/y}$-hyposensitive mice. Thus, E/I ratio alterations lead to a noisier network[51–53] in $Fmr1^{-/y}$-hyposensitive mice in a context-dependent manner, which might explain reduced stimulus detection through a decreased signal-to-noise ratio in non-detected trials.

Unreliable stimulus encoding impedes response decoding in $Fmr1^{-/y}$-hyposensitive mice

To further explore the differences in the transformation of the perceptual magnitude into a behavioral response (response decoding) between WT and $Fmr1^{-/y}$-hyposensitive mice, we employed dynamic decoding classifiers using a logistic regression model. We trained the model on each acquisition frame (32 ms) during the pre-stimulus (1s) and stimulus-related (500 ms) neuronal activity of each mouse[50], to predict stimulus detection based on neuronal activity (Fig. 4a). In WT mice, our model successfully differentiated detected from non-detected trials (Fig. 4b). However, it performed worse when trained with datasets of $Fmr1^{-/y}$-hyposensitive mice (Fig. 4c). Comparisons of the decoding accuracy during stimulus delivery between the two groups showed a strong trend for less accurate predictions of detected trials in $Fmr1^{-/y}$-hyposensitive mice (Fig. 4d). This effect was exacerbated when comparing the accuracy of the model during the last 250 ms of the stimulus (Fig. 4e), an approach that considers evidence accumulation during stimulus delivery[54].

We previously saw that pre-stimulus neuronal activity impacts stimulus-related responses, with the variability of pre-stimulus activity positively correlating with stimulus-related TBT variability in WT mice (Fig. 3i). We thus calculated the decoding accuracy of our model during the last 200 ms of the pre-stimulus period, close to stimulus onset. We observed a performance above chance level in predicting detected stimuli in WT mice, but not in $Fmr1^{-/y}$-hyposensitive mice (Fig. 4f), confirming that pre-stimulus activity influences stimulus detection in WT mice.

To investigate the origin of the decreased decoding accuracy in $Fmr1^{-/y}$-hyposensitive mice, we examined the impact of TBT variability of neuronal responses on decoding accuracy. We found a positive correlation between TBT similarity and model accuracy in WT mice and a strong trend in $Fmr1^{-/y}$-hyposensitive mice (Fig. 4g). In contrast, the accuracy of the model did not correlate with the number of recruited neurons (Fig. 4h) or that of reliable responders (Fig. 4i), indicating that the model did not rely on the number of neurons responding to stimulation to predict the

behavioral outcome. These results show that increased TBT variability impacts response decoding, rendering it less accurate in *Fmr1*$^{-/y}$-hyposensitive mice.

Altogether, our results show reliable response decoding based on perceptual magnitude and influenced by pre-stimulus activity in WT mice. In contrast, increased TBT variability in *Fmr1*$^{-/y}$-hyposensitive mice impedes response decoding, highlighting the impact of the ongoing network state in stimulus detection and suggesting a mechanistic feature underlying poor behavioral performance in *Fmr1*$^{-/y}$-hyposensitive mice.

Tactile sensitivity is improved upon treatment with a BK_{CA} agonist in *Fmr1*$^{-/y}$ mice

Large conductance voltage- and calcium-sensitive potassium (BK_{Ca}) channel dysfunction has been associated with neurodevelopmental conditions such as autism and fragile X syndrome[55–57]. Administration of BK_{Ca} channel agonists can improve certain neuronal and behavioral alterations in *Fmr1*$^{-/y}$ mice[27,49,58,59]. However, whether sensory perception can be corrected by BK_{Ca} channel openers, and how restoring neuronal function by increasing BK_{Ca} channel opening probability can contribute to behavioral improvements is currently unknown. To probe the correction of tactile hyposensitivity of *Fmr1*$^{-/y}$ mice (both typically detecting and hyposensitive, Fig. 1b-c), we delivered the brain blood barrier permeable BK_{Ca} channel agonist, BMS-204352 (BMS), or its vehicle via intraperitoneal injection, as described previously[58,59], 30-45 minutes before tactile detection testing.

Our results demonstrate that increasing the probability of BK_{Ca} channel opening in a voltage- and calcium-dependent manner improved tactile sensitivity in *Fmr1*$^{-/y}$ mice (Fig. 5a-c), which showed similar detection thresholds to their WT littermates (Fig. 5d). Treatment also eliminated the difference in the perceptual accuracy between the groups (Fig. 5e), but did not affect the licking strategy (Fig. 5f). Our results demonstrate that decreasing excitability by shifting the dynamics of BK_{Ca} channel opening improves perceptual thresholds in *Fmr1*$^{-/y}$ mice.

Treatment with a BK_{CA} agonist enhances stimulus encoding in *Fmr1*$^{-/y}$ mice

We then used the same pharmacological strategy to test if we could validate our findings of the neuronal underpinnings of atypical tactile perception in autism. To examine whether stimulus encoding in *Fmr1*$^{-/y}$ mice (both typically detecting and hyposensitive) was improved following BMS-204352 administration, we analyzed neuronal responses during our vibrotactile detection task. Indeed, BMS-204352 treatment enhanced stimulus encoding in *Fmr1*$^{-/y}$ mice (Fig. 5g) by increasing the number of activated pyramidal neurons during detected trials, reducing the difference between WT and *Fmr1*$^{-/y}$ mice (Fig. 5h-top). No change was observed in the percentage of activated GABAergic interneurons (Fig. 5h-bottom) or inhibited neurons (Fig. S4a).

We assessed the strength of the perceptual magnitude during detection by calculating the difference in the number of recruited neurons between detected and non-detected trials. Remarkably, under BMS treatment the differentiation of detected and non-detected trials was similar in *Fmr1*$^{-/y}$ and WT mice. This was evidenced by the percentage of activated pyramidal neurons and GABAergic interneurons (Fig. 5i) and the percentage of inhibited GABAergic interneurons (Fig. S4b). Moreover, the number of activated pyramidal reliable responders in detected trials was similar between *Fmr1*$^{-/y}$ and WT mice upon pharmacological treatment (Fig.

5j). No difference was observed in the number of recruited neurons during non-detected trials between WT and *Fmr1*$^{-/y}$ mice (Fig. S4c).

We then examined if BMS treatment modulated TBT variability of suprathreshold responses at the neuronal network level during tactile perception. In agreement with previous results on the amplitude of subthreshold responses[49], we didn't find reduced TBT variability in neuronal activity (z-score) upon BMS treatment in *Fmr1*$^{-/y}$ mice. We found, instead, a surprising trend for increased TBT variability (Fig. S4d), further confirmed by high TBT variability in the activity of non-reliable responders upon stimulation (Fig. S4e).

Collectively, our results show that BMS treatment enhanced stimulus encoding, enabling a better differentiation between detected and non-detected trials in *Fmr1*$^{-/y}$ mice. This allowed a stronger and more reliable perceptual magnitude to determine response decoding and render it less contingent upon the network state, even though the latter became more variable.

Discussion

In this study, we tackled the challenge of experimentally mimicking the nuanced and heterogeneous features of atypical sensory perception reported in autistic individuals in a transgenic mouse model, by back-translating a psychophysical task used in human studies[60]. Our results demonstrate a remarkable fidelity in capturing the nuances of altered sensory perception in autism, such as tactile hyposensitivity[12,13], high interindividual variability[18,28,30,31], unreliable responses[8,41,42], and hypo-responsiveness[7,10]. Consistent with human studies[61,62], these tactile symptoms were not linked with cognitive deficits.

Tactile perception alterations in autism depend both on the tactile sub-modality and the body part that receives the stimulus, revealing hypo- or hypersensitivity in autistic individuals[12,13,15]. Our findings of tactile hyposensitivity in *Fmr1*$^{-/y}$ mice are consistent with studies of the same mouse model using forepaw-dependent discrimination tasks[63,64] and show the importance of the tactile sub-modality in behavioral responsivity[65]. Similarly, our findings underline the importance of the stimulated body part as, for example, whisker stimulation revealed hypersensitivity in the *Shank3B*$^{-/-}$ mouse model[22] and hyper-responsiveness in *Fmr1*$^{-/y}$ mice[66].

Intriguingly, we reveal a subgroup of *Fmr1*$^{-/y}$ mice with tactile hyposensitivity. This result was unexpected for an inbred mouse line but supports the existence of sensory subgroups with different tactile features in autism[62] and underlines the relevance of addressing inter-individual variability in autism research. The increased body weight of the hyposensitive-*Fmr1*$^{-/y}$ subgroup suggests that metabolic alterations in autism[36–40,67–69] might impact the metabolic rate of the neocortex and thus tactile sensitivity[34,35].

We linked our psychophysical task with measures of neuronal circuit activity to reveal the neocortical substrates underlying forepaw-dependent tactile detection. We show that the role of the forelimb-related primary somatosensory cortex in tactile detection in humans[70–72] is evolutionarily conserved in mice. We demonstrate that encoding of vibrotactile stimuli within the S1-FP of mice generates perceptual magnitudes through both activation and inhibition of pyramidal neurons. This is consistent with a recent study of stimulus encoding in the visual cortex of mice showing that perceptual magnitude is produced through both activation and inhibition

of neuronal ensembles[73]. Our findings show that recruitment of small neuronal subsets (on average 10% of the neuronal population) in FP-S1 is sufficient to lead to detection[74], expanding the notion of sparse stimulus encoding and revealing a role for sparse neuronal inhibition during stimulus detection.

A previous study suggested that stimulus detection depends on the signal-to-noise ratio in S1[50]. Here we confirm this, showing that the perceptual magnitude generated through the encoding of detected stimuli was stronger from that of non-detected ones. We demonstrate that during ambiguous threshold stimuli, detection depends on the number of activated pyramidal neurons. We further validate that noise or variability in S1 affects detection[50,75], evidenced by the effect of prestimulus activity in stimulus encoding and response decoding. Finally, our model shows that neuronal responses in the FP-S1 during stimulation are sufficient to decode the behavioral response to the stimulus, congruent with results from the barrel cortex[76,77].

We reveal that weak and unreliable stimulus encoding in *Fmr1*$^{-/y}$-hyposensitive mice generates a low perceptual magnitude and makes response decoding highly contingent upon the ongoing network state. We demonstrate that activation of GABAergic neurons is reduced during non-detected trials in *Fmr1*$^{-/y}$ mice, increasing the E/I ratio, an indicator of the balance in the network state, which might contribute to reduced perceptual sensitivity. Increased E/I ratio was previously shown in autistic individuals and mouse models of autism[20,51,78], and decreased GABA levels have been correlated with decreased sensitivity during tactile perception[19].

Reduced somatosensory responses were previously reported in autistic individuals[17,18] and in the *Syngap1*$^{+/-}$ mouse model of autism, where they were linked to reduced synaptic connectivity and impaired intrinsic excitability[79]. However, *Fmr1*$^{-/y}$ mice show circuit hyperexcitability in primary sensory cortices[49,58,80]. We speculate that perceptual magnitude is dampened and tactile detection is undermined in *Fmr1*$^{-/y}$-hyposensitive mice due to neocortical hyperexcitability and its effect on canonical computations, like divisive normalization[81]. In this scenario, hyperexcitability in FP-S1 in *Fmr1*$^{-/y}$ mice would reduce the signal-to-noise ratio during stimulation, with the stimulus-related information that arrives in each neuron being normalized over the non-stimulus-related inputs that rise from the hyperexcitable network. This would result in a decreased number of stimulus-recruited neurons in *Fmr1*$^{-/y}$-hyposensitive mice and an increased response variability that depends on the ongoing network state and has been proposed as a hallmark of autism[44,45,49,82,83]. Using dynamic decoding classifiers, we show that this variability impacts response decoding, making it less predictable.

Administration of a BK_{Ca} channel agonist[27,49,58,59,84] ameliorates tactile detection in *Fmr1*$^{-/y}$ mice by strengthening the perceptual magnitude and its reliability. While most of the previous studies have investigated the therapeutic benefit of constitutively activating $GABA_B$ receptors[85–87], here we showed a novel approach to manipulate network dynamics, by decreasing excitability. We speculate that reduced spontaneous firing activity upon treatment[49] increases the signal-to-noise ratio via enhancement of the weight of the stimulus-related input at the S1-FP neurons. Similar to previous results on the trial-by-trial variability in the amplitude of subthreshold responses in anesthetized *Fmr1*$^{-/y}$ mice[49], we did not observe a decrease in the trial-by-trial variability of suprathreshold responses at the neuronal network level in behaving mice.

We reveal a surprising tactile heterogeneity in perceptual and neuronal responses in a mouse model of autism and demonstrate that tactile hyposensitivity stems from weak and unreliable stimulus encoding in the primary somatosensory cortex. This renders response decoding more vulnerable to the noisy network state and thus less predictable. Our work advocates for subject classification into subgroups based on sensory features, both in human studies[62,88,89] and in preclinical models of autism. This stratification is crucial for evaluating novel treatments in preclinical and clinical studies, facilitating personalized treatment[90]. Finally, our experimental platform can be extended to other neurodevelopmental and psychiatric disorders where sensory features are prevalent, including ADHD, sensory processing disorder, and schizophrenia[91].

Materials and Methods

Experimental design

We back-translated a task used in human studies[12,13] and developed a novel Go/No-go detection task for vibrotactile stimuli which we combined with two-photon calcium imaging of excitatory and inhibitory neurons in the forepaw-related primary somatosensory cortex (FP-S1) to study altered tactile perception in autism and define its neural correlates. Throughout the text, we are using terms that are preferred in the autistic community and are less stigmatizing.

Ethical statement

All experimental procedures were performed in accordance with the EU directive 2010/63/EU and French law following procedures approved by the Bordeaux Ethics Committee and Ministry for Higher Education and Research. Mice were maintained in reversed light cycle under controlled conditions (temperature 22–24 °C, humidity 40–60%, 12 h/12 h light/dark cycle, light on at 21:00) in a conventional animal facility with ad libitum access to food and ad libitum access to water before the water restriction period. All experiments were performed during the dark cycle, under red light.

Mice

Second-generation *Fmr1* knockout (*Fmr1*$^{-/y}$) and wild-type littermate mice, 5-16 weeks old, were used in our study. Mice were fully congenic, with a C57Bl/6J background (backcrossed for more than 10 generations into C57Bl/6J). Male wild-type and *Fmr1*$^{-/y}$ littermates were generated by crossing *Fmr1*$^{+/-}$ females with *Fmr1*$^{+/y}$ male mice from the same production, and the resulting progeny used for our experiments was either *Fmr1*$^{+/y}$ (wild type) or *Fmr1*$^{-/y}$ (KO). Mice were maintained in collective cages following weaning (2-4 litter males per cage). Cages were balanced for genotype and supplemented with cotton nestlets and carton tubes. Number of mice are given in the figure captions. The genotype of experimental animals was re-confirmed post hoc by tail-PCR.

Surgery

Mice (P33-42) were anaesthetized with isoflurane (4.5% induction, 1.5-2% maintenance). Proper depth of anesthesia was monitored by testing the absence of a foot-pinch reflex and whisker

movement. Mice were head-fixed using non-puncture ear-bars and a nose-clamp, and optic gel (Ocry-gel) was applied to both eyes. Body temperature was maintained at 37 °C with a heating pad and rectal probe. Before the surgery, saline (0.1 ml/ 10 g) and 0.1 ml of a 1:10 Buprenorphine to saline solution were administered subcutaneously. Following hair trimming and application of Betadine scrub and Betadine dermal solution at the scalp, 0.1 ml of a 1:4 Lidocaine to saline solution was administered subcutaneously and waited for 2–5 min to induce local analgesia. The scalp was carefully removed and a 3 mm diameter craniotomy was made above the S1 forepaw region (0.75 mm anterior and -2.5 mm lateral from Bregma, confirmed with intrinsic imaging coupled with forepaw stimulation) using a dental drill (World Precision Instruments). The cortical surface was rinsed with saline throughout the surgery. Stereotactic injections of 100 nl of AAV1/2-syn-jGCaMP8m (titer: 2.6E+12 gcp/ml, diluted 1:4 in Hank's Balanced Salt Solution) and AAV1/2-mDlx-HBB-chI-mRuby3-SV40p(A) (titer: 8.6E+13 gcp/ml, diluted 1:2 in Hank's Balanced Salt Solution) were delivered (50 nl/ min) in layers 2/3 (z depth 0.3mm). A double coverslip, composed of a 3 mm diameter lower glass and a 4 mm diameter upper glass glued together with optical adhesive (NOA 61, Norland Products), was implanted on top of the craniotomy and secured in place with cyanoacrylate glue. A head-post was attached to the skull with cyanoacrylate glue and secured with dental cement. An optical glue (OptiBond Universal, Kerr) and dental filling material (Charisma, Kulzer) were applied to the skull and curated with LED blue light. Dental cement was applied on the top. After the surgery the mice were placed on a warm blanket for 1 h after they awoke from anesthesia.

Go/No-Go vibrotactile decision-making task

Setup

The vibrotactile decision-making setup was positioned in an isolation cubicle to minimize interference during the experiment. Mice were placed in a body tube and were head-fixed with their forepaws resting on two steel bars (6 mm diameter, Thorlabs). The right bar was mounted to a Preloaded Piezo Actuator (P-841.6, Physik Instrumente) equipped with a strain gauge feedback sensor and controlled (E-501, Physik Instrumente) in a closed loop, as described before[92]. Water reward was delivered through a metal feeding needle (20G, 1,9mm tip**,** Agntho's AB) connected to a lickport interface with a solenoid valve (Sanworks) equipped with a capacitive sensor (https://github.com/poulet-lab/Bpod_CapacitivePortInterface). The behavioral setup was controlled by Bpod (Sanworks) through scripts in Python (PyBpod, https://pybpod.readthedocs.io/en/latest/).

Habituation to head-fixation and water restriction

Mice (P40-P50) were handled using carton tubes and the cupping technique until they were comfortable in the experimenter's hands, attested by eating while handled. Mice were gradually habituated to the experimental setup and head fixation for 5 days. On the third day of habituation, a water-restriction protocol was implemented, where mice had access to liquid water in the setup and to a solid water supplement (Hydrogel, BioServices) in their home cage. In total, the animals received 1.5-2 ml of water per day, which corresponds to 50-65% of their ad libitum consumption, while ensuring that they did not lose more than 10% of their weight. Each

mouse received 6-8 g of Hydrogel (ad libitum) during the weekend. This water restriction protocol was maintained throughout behavioral training and until the end of behavioral testing.

Go/No-Go vibrotactile task training and testing

Habituated mice (8 weeks old) were trained to associate vibrotactile stimulus delivery (pure sinusoid, 500 ms duration, 15 µm amplitude, 40 Hz frequency) with a water reward (8 µl). Go trials consisted of stimulus delivery followed by a 2 s response window during which the mice could lick to receive the reward. No-Go (catch) trials included no stimulation and licking during these trials resulted in a 5 s timeout before the beginning of the following trial. Inter-trial intervals were variable (5-10 s). The training was subdivided into 3 phases: (a) automatic water delivery at the beginning of the response window (b) Pre-training: lick-triggered water delivery during Go trials and timeout delivery during No-Go trials (c) Training: lick-triggered water delivery during Go trials when the mouse did not lick during the inter-trial interval (3-8 s) before the stimulation. No stimulus delivery and timeout (5 s) if the animal licked during the inter-trial interval (3-8 s) before the stimulus and timeout delivery (5 s) during No-Go trials. All sessions consisted of 300 trials with 70-80% Go and 20-30% No-Go proportion. All trials were presented in a pseudorandom sequence. Pilot experiments with an extra sensor to monitor forepaw placement confirmed that the mice did not remove their forepaws from the bar before stimulus delivery. To complete Pre-training, mice needed to complete 80% of successful Go trials and reduce their spontaneous licking during No-Go trials below 40%. To complete Training, mice needed to reach the criterion of more than 80% successful Go-trials and less than 30% unsuccessful No-Go trials as an average for 3 consecutive days. All mice that fulfilled this criterion were tested for the detection of vibrotactile stimuli of differing amplitudes that they haven't experienced before. During testing a 90% Go:10% No-Go ratio was delivered. Go trials consisted of 6 vibrotactile stimuli (pure sinusoid, 500 ms duration, 10 Hz frequency, 2-4-6-8-10-12 µm amplitude), delivered in a pseudorandom manner.

Go/No-Go vibrotactile task analysis

All analysis was performed with custom-made Python scripts. Behavior was quantified based on the lick events and four main outcomes were measured: Hit and Miss rate for successful and unsuccessful Go trials respectively (number of Hit or Miss divided by the total number of Go trials where a stimulus was delivered), Correct Rejection and False Alarm rate for successful and unsuccessful No-Go trials respectively (number of Correct Rejections or False alarms divided by the total number of No-Go trials). Prestimulus spontaneous licking was calculated as Timeout events during Go trials divided by the total number of Go trials. Training duration was calculated based on the total number of days each animal passed in pre-training and training. For testing, only sessions with less than 40% unsuccessful No-Go trials were analyzed. Psychometric curves were fitted on the Hit rate for each stimulus amplitude using a general linear model. An average of 140 repetitions for each amplitude was used to calculate Hit rates. Detection thresholds were calculated based on the psychometric curves, as the stimulus amplitude at the inflection point of the sigmoid fitting curve. Accuracy was calculated based on the slope of the psychometric curve. Relative criterion was calculated as:

$$c' = \frac{-1}{2}\frac{\big(z(Hit) + z(FalseAlarm)\big)}{\big(z(Hit) - z(FalseAlarm)\big)}$$

(Detection Theory[93]).

where z(Hit) is the standard deviation unit for the Hit rate and z(False Alarm) is the standard deviation unit for the False Alarm rate.

Trial-by-trial variability

Trial-by-trial variability of behavioral responses was measured based on the variance of Hit responses during Go trials for each stimulus amplitude. Low variance of Hit responses thus corresponds to consistently detected or non-detected stimulus amplitudes. Normalized trial-by-trial variability was calculated for the threshold (x) amplitude of each mouse, the first amplitude after the threshold (x + 2 µm, suprathreshold), and the first amplitude before the threshold (x - 2 µm, subthreshold).

Clustering of *Fmr1*$^{-/y}$ mice in subgroups

The sci-kit learn implementation of k-means was used on the Hit rates of *Fmr1*$^{-/y}$ mice across all stimulus amplitudes, with 2 clusters targeted and the default parameters.

Adhesive tape removal test

Mice (11-13 weeks old) were handled for one day and underwent three days of gradual habituation to restriction and a round Plexiglas arena (14 cm diameter). Two patches of adhesive tape were attached to their forepaws as described before[46]. The time before the first contact of each tape and the total time necessary for their removal were calculated manually using a Python script.

Two-photon calcium imaging

Setup

Calcium measurements were performed using a Femtonics FEMTOSmart microscope coupled with a widely tunable, femtosecond Ti:Sapphire Laser (Chameleon Ultra, Coherent) pumped by a solid-state laser (Verdi 18W, Coherent). Excitation at 920 nm was used for GCaMP8m and at 1000 nm for mRuby3 and two photomultiplier tubes were used for the collection of green and red fluorescence. Laser power was modulated using a Pockels cells A 20x/1 NA objective (Zeiss) was used to obtain 512 × 512-pixel images covering 480 × 480 µm of cortex were acquired at 30.96 Hz using the resonant scanner system (Femtonics). Measurements were written as a series of 32-bit images and saved as ome files. Analog and digital inputs sent by Bpod and the piezoelectric sensor controller were collected and saved as timestamps by the microscope and were used to synchronize the behavioral events with the calcium traces from imaging.

Analysis

Measurements were exported in ome files of 2000 frames and converted into tiff files using Fiji (ImageJ). Motion correction, region of interest (ROI) detection and fluorescence extraction were performed using Suite2p (https://suite2p.readthedocs.io/en/latest/index.html) with standard parameters, double registration and denoising. The selection of neurons as ROIs was confirmed through manual curation of the identified ROIs based on shape and calcium traces. To define the inhibitory neurons, colocalization of images obtained for green and red fluorescence was performed using ImageJ. All further analyses were performed separately for excitatory and inhibitory neurons. Custom-made scripts were written in Python to synchronize the behavioral and imaging data and to calculate ΔF/F and z-score values. Neuropil contamination was corrected in all traces before ΔF/F and z-score calculations as:

$$F_{neuropil\text{-}corrected} = F - F_{neuropil} * 0.7.$$

where F is the fluorescence of the neuron (ROI) and $F_{neuropil}$ is the fluorescence of the neuropil associated with the neurons, as calculated by suite2p.

To calculate ΔF/F, baseline fluorescence (F) was calculated for each neuron as the average fluorescence during the 10 s period with the lowest variation (STD) in F.
z-scores were calculated as:

$$z(t) = \frac{\Delta F/F\ (t) - \mu_{prestimbaseline}}{\sigma_{prestimbaseline}}$$

where $\mu_{prestim\ baseline}$ is the mean ΔF/F during the 1 s before stimulation across all trials and $\sigma_{prestim\ baseline}$ is the standard deviation ΔF/F during 1 second before stimulus

All analysis of stimulus-specific responses was conducted in the time window that the stimulus was present, but before the animal's first lick to avoid confounding stimulus- with movement-related activity.

Stimulus-related responses

Stimulus-related activation of a given neuron was computed for each trial by comparing the 85th percentile of the z-score during stimulation to 1,999 random points in the recording (z-score), excluding periods where the stimulus or a reward was delivered. When the z-score during stimulus delivery was higher than the 95th percentile of the 1,999 random points, the neuron was consider activated by the stimulus. A similar method was used for stimulus-related inhibition, comparing the 10th percentile of the z-score during stimulation with 1,999 random points in the recording (z-score). The neuron was considered inhibited by the stimulus if the z-score was lower than -1 * 95th percentile of the 1.999 points. This procedure was adapted from ref[92] constitutes a randomization test at significance level $P < 0.05$.

Response characterization (peak amplitude, peak delay)

Response amplitude was calculated for all neurons that were activated or inhibited during stimulus delivery as the maximum or minimum z-score value during the 500 ms of stimulation. The peak delay was defined as the number of frames between the beginning of stimulus delivery and the peak response amplitude.

Prestimulus activity analysis

Prestimulus activity was calculated as the mean or STD of the z-score, during the 500 ms window before stimulus onset.

Trial-by-trial variability

To estimate the trial-by-trial variability, cosine similarity was calculated between each pair of trials. Trials were represented as vectors. Each neuron was assigned a value of the average z-score fluorescence during stimulus delivery (500 ms) or of its response with the following labels: activated (1), inhibited (-1), or non-responsive (0). Cosine similarity of prestimulus responses was calculated with each neuron assigned a value of its average z-score fluorescence during 500 ms before stimulus onset. For group comparisons, the pair-wise matrices were averaged to one single value of cosine similarity for each animal.

Reliable responders

Neurons were defined as reliable responders if they were recruited (activated or inhibited) more than 5 times during detected trials.

Excitation-inhibition (E/I) ratio

E/I ratio was calculated for each trial as the number of activated pyramidal neurons divided by the number of activated GABAergic interneurons.

Decoding of behavioral responses

Dynamic decoding classifiers were adapted from ref.[50], using a logistic regression (Scikit-learn implementation) model with an L2 penalty term to the weights with a regularization strength of 1. Classification accuracy was computed for each frame, with shaded areas showing the SEM. Decoding accuracy for different time windows was calculated by averaging the accuracy of the frames that constitute each time window across trials. The random undersampling method was used to balance the number of detected/undetected trials, because of the altered Hit/Miss ratio in WT and *Fmr1*$^{-/y}$ mice (Scikit-learn library). This method keeps random trials of the majority class to obtain the same number of trials as in the minority class. Each model was trained in each mouse, to classify the probability of a trial having a Hit or Miss outcome. Four-fold cross validation was used on each session, with a new model trained for each fold for each time-point, and

classification accuracy is reported as the average of the test data across folds. A new model was trained from scratch for each imaging frame within a trial; hence, the training data consisted of a vector containing a single scalar ΔF/F value for each cell of all trials on a given frame.

Pharmacology

For rescue experiments, vehicle (standard saline solution, 0.9 M NaCl, supplemented with 1.25% DMSO and 1.25% Tween 80) or BMS-204352 (2 mg per kg, Tocris) were delivered by intraperitoneal injection 30 min before behavioral testing (as described previously Zhang). All mice were first habituated to restriction. Each mouse was treated for 2 days with the vehicle and for 2 days with BMS-204352. Testing in the Go/No-Go vibrotactile decision-making task occurred 30 minutes after each treatment, on both days. All sessions were included in the analysis (no criterion for sessions with less than 40% unsuccessful No-Go trials was employed).

Histology

Following the end of the experiments, mice were anesthetized with isoflurane (4.5%) and euthanized by cervical dislocation. The brain was extracted, fixed in PFA 4% overnight, and washed in 0.1 M PB. Coronal brain slices of 100 mm thickness were obtained using a vibrotome (Leica VT1000 S). Slices were stained with DAPI and the localization of the virus injection in the forepaw-related primary somatosensory cortex was confirmed in a fluorescent microscope (Eclipse Ti-U Nikon).

Statistics

All values are presented as mean ± s.e.m. Box plots show the median, interquartile, range, mean and individual values. The numbers of animals used are indicated in the figure legends. All statistical analysis was done using Python (SciPy, Pingouin). All datasets were tested for normality. Two-tailed unpaired or paired *t*-tests were performed to evaluate the difference between two groups of data. When normal distribution was not confirmed, Mann-Whitney U test was used for comparisons between different groups and Wilcoxon Signed Rank test was used for within-group comparisons. Genotype effects were tested with one-way ANOVA or Kruskal-Wallis ANOVA when more than two groups were present. Genotype and Amplitude or Variance effects were tested with Mixed ANOVA or the Friedman test was used for repeated measures analysis.

Blinding and randomization

All experiments and analyses were performed in a blinded manner. Although no randomization was formally applied, the subjects were indeed selected at random due to the blinded nature of the experiments. For pharmacological rescue experiments, equal numbers of *Fmr1*$^{-/y}$ and wild-type mice received BMS-204352 or vehicle. Treatments were evenly assigned within a littermate group.

Code availability

Custom-made Python codes used in this study can be found on the following GitHub repository: https://github.com/OuraniaSem/Percephone.git

Data availability

The raw data of behavioral experiments and calcium imaging generated in this study have been deposited on the figshare database: https://doi.org/10.6084/m9.figshare.26335684.v2
Source data are provided with this paper.

Figures and Figure Legends

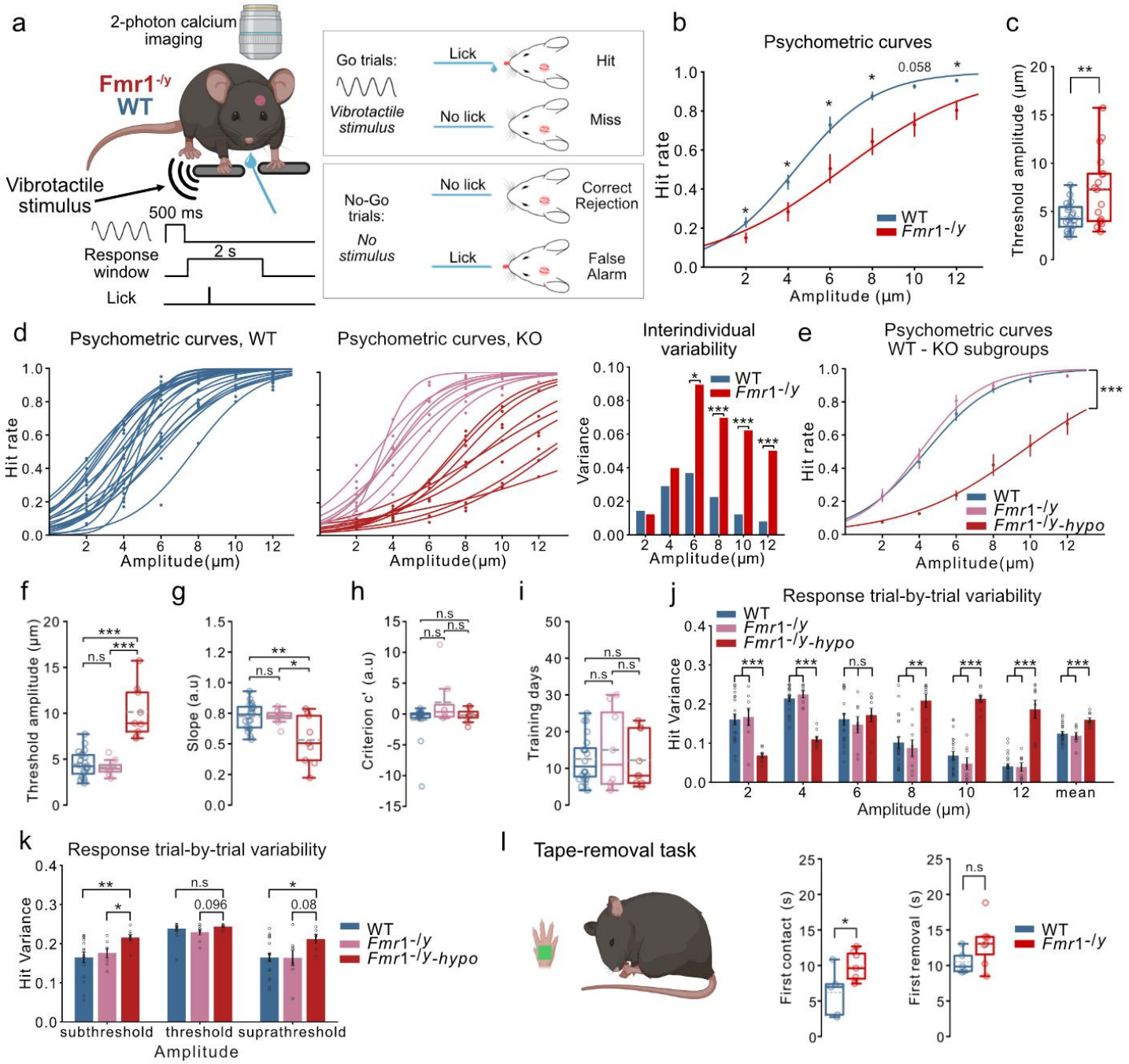

Figure1. **A forepaw-based perceptual decision-making task to assess tactile detection in mice.**

For panels **b, c, d, e, f, g, i, j,:** n=20 WT, 17 *Fmr1*$^{-/y}$ mice (of which 9 *Fmr1*$^{-/y}$-hyposensitive), 5-7 sessions with ~130 repetitions of each amplitude per mouse. For panel **h,:** n=19 WT, 8 *Fmr1*$^{-/y}$, 8 *Fmr1*$^{-/y}$-hyposensitive mice. For panel **k,:** subthreshold: n=16 WT, 7 *Fmr1*$^{-/y}$, 9 *Fmr1*$^{-/y}$-hyposensitive mice, threshold: n=20 WT, 8 *Fmr1*$^{-/y}$, 8 *Fmr1*$^{-/y}$-hyposensitive mice, suprathreshold: n=20 WT, 8 *Fmr1*$^{-/y}$,6 *Fmr1*$^{-/y}$-hyposensitive mice. For panel **l,:** n=5 WT, 7 *Fmr1*$^{-/y}$ mice. **a,** Left: schema showing the behavioral setup and trial protocol. Right: behavioral outcomes depending on the animal's response. **b,** Psychometric curves fitted on average Hit rates for each stimulus amplitude and **(c,)** Detection thresholds calculated based on the psychometric curves. **d,** Psychometric curves of each individual mouse (left and middle, colors depict different groups) and variance of Hit rates (right). **e,** Psychometric curves fitted on average Hit rates for each stimulus amplitude for WT mice and the two Fmr1$^{-/y}$ subgroups. Detection thresholds **(f,)** and perceptual accuracy **(g,)** calculated based on the psychometric curves in **(e,). h**, Relative criterion c' depicting the licking strategy. **i,** Number of days mice spent in pre-training and training. **j,** Trial-by-trial variability calculated as response variance of Hit for each stimulus amplitude and the average for all amplitudes. **k,** Trial-by-trial variability (variance) of Hit responses following normalization for the threshold amplitude of each mouse. Subthreshold stimulus is the first stimulus with amplitude lower than the threshold and suprathreshold stimulus is the first amplitude higher than the threshold. **l,** Left: schema showing the tape removal task. Right: Time (s) until the first contact with the tape and time (s) until the tape removal. P values were computed using Mixed ANOVA for panels **b, e,;** one-way ANOVA for panels **f,-g,;** Kruskal-Wallis ANOVA for panels **h,i,;** Friedman test for panels **j,k,;** two-sided t-test for panels **c, e, f, g, i, j, k, l,**; Mann-Whitney test for panels **b, e, h, i, j, k,**; F test for panel **d**,. ***P < 0.001, **P < 0.01, *P < 0.05 or n.s, not significant.

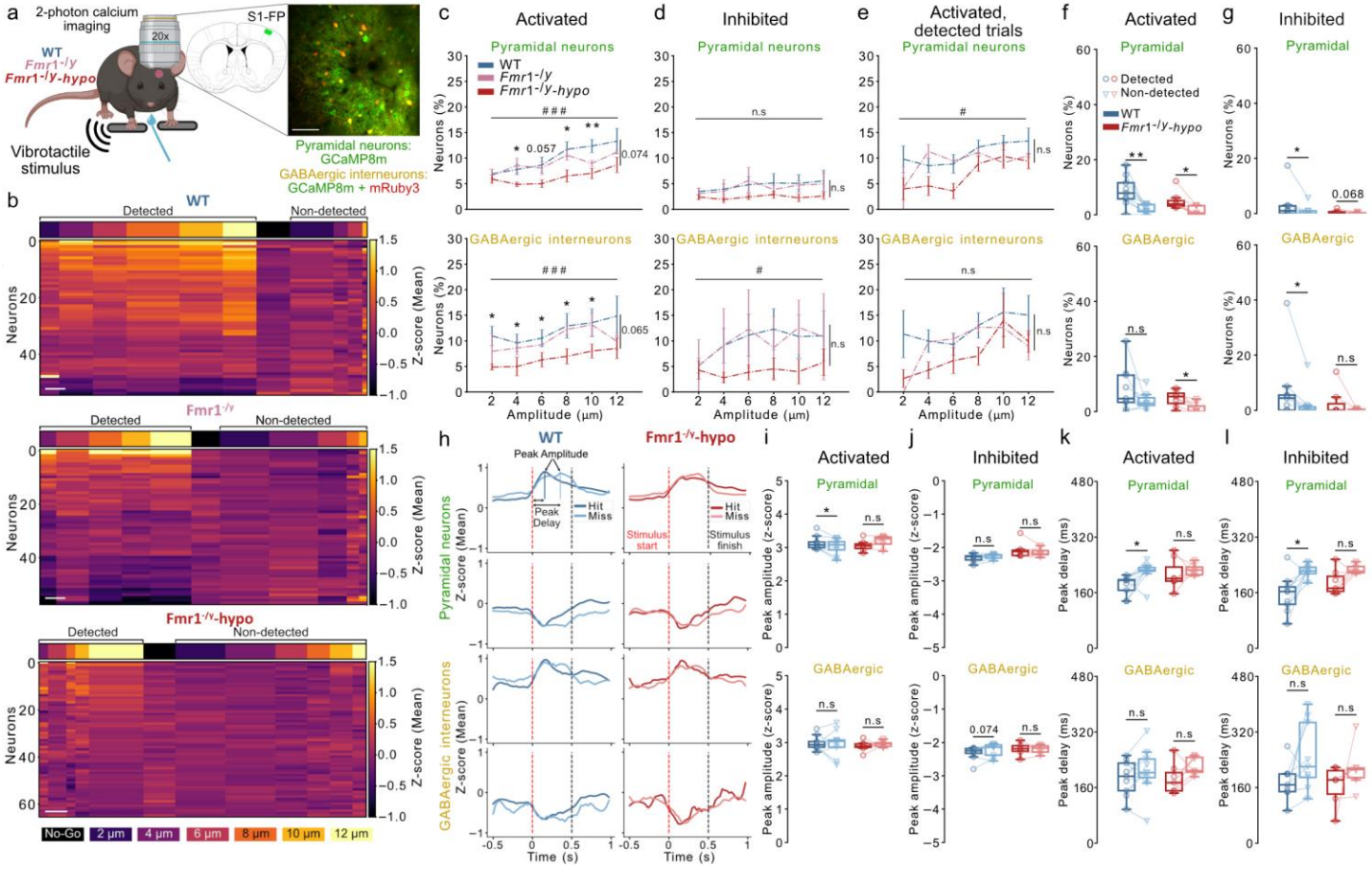

Figure 2. **Weak stimulus encoding in *Fmr1*$^{-/y}$-hyposensitive mice**

For all panels: 1 session, ~10 repetitions of each amplitude per mouse. For panels **c, d, e,:** n=9 WT, 2 *Fmr1*$^{-/y}$ mice, 7 *Fmr1*$^{-/y}$-hyposensitive mice. For panels **f,-k,** (Pyramidal neurons): n=9 WT, 7 *Fmr1*$^{-/y}$-hyposensitive mice. For panels **h, j**, (GABAergic interneurons): n=8 WT, 7 *Fmr1*$^{-/y}$-hyposensitive mice. For panels **i, k,** (GABAergic interneurons): n=9 WT, 6 *Fmr1*$^{-/y}$-hyposensitive mice. **a,** Left: schema showing the imaging setup during tactile detection. Right: Position of injections in the forepaw-related primary somatosensory cortex and example of the field of view (scale bar: 100 mm). GCaMP8m is expressed by excitatory pyramidal neurons and inhibitory GABAergic interneurons. Inhibitory neurons also co-express the red fluorescent marker mRuby3. **b,** Example heat maps of activity (z-score) during stimulus delivery for one WT, one *Fmr1*$^{-/y}$, and one *Fmr1*$^{-/y}$-hyposensitive mouse. Each horizontal line depicts a neuron. Vertical lines show averaged activity across trials for each stimulus amplitude. Stimuli are sorted depending on their amplitude and whether they were detected (left) or not (right). No-Go trials are shown in the middle (black). Color-coding of each amplitude is shown at the bottom. (scale bar: 5 trials) **c,** Average percentage of activated pyramidal neurons (top) and GABAergic interneurons (bottom) for each stimulus amplitude. **d,** Same as (**c,**) but for inhibited neurons. **e,** Same as (**c,**) but for activated neurons during detected trials. **f,** Percentage of activated pyramidal neurons (top) and GABAergic interneurons (bottom) in detected (dark color, circles) and non-detected (light-color, triangles) trials. **g,** Same as (**f,**) but for inhibited neurons. **h, C**alcium traces of neuronal responses averaged across trials and mice. Z-score responses of pyramidal neurons and GABAergic interneurons before, during, and after stimulation during detected (Hit) and non-detected (Miss) trials are shown. Peak amplitude and peak delay are indicated. **i,** Quantification of peak response amplitude (z-score) of activated pyramidal neurons (top) and GABAergic interneurons (bottom). **j,** Same as (**i**,) but for inhibited neurons. **k,** Quantification of response delay (ms) of the peak amplitude relative to stimulus onset for activated pyramidal neurons (top) and GABAergic interneurons (bottom). **l,** Same as (**k,**) but for inhibited neurons. P values were computed using a mixed ANOVA for panels **c, d, e,**; two-sided t-test for panels **c, d, e,**; two-sided paired t-test for panel **f, i, j, k, l,**; Wilcoxon signed-rank test for panels **f, g, i, j, k**. $^{###}$P < 0.001, $^{\#}$P < 0.05, for amplitude effect. **P < 0.01, *P < 0.05 or n.s, not significant.

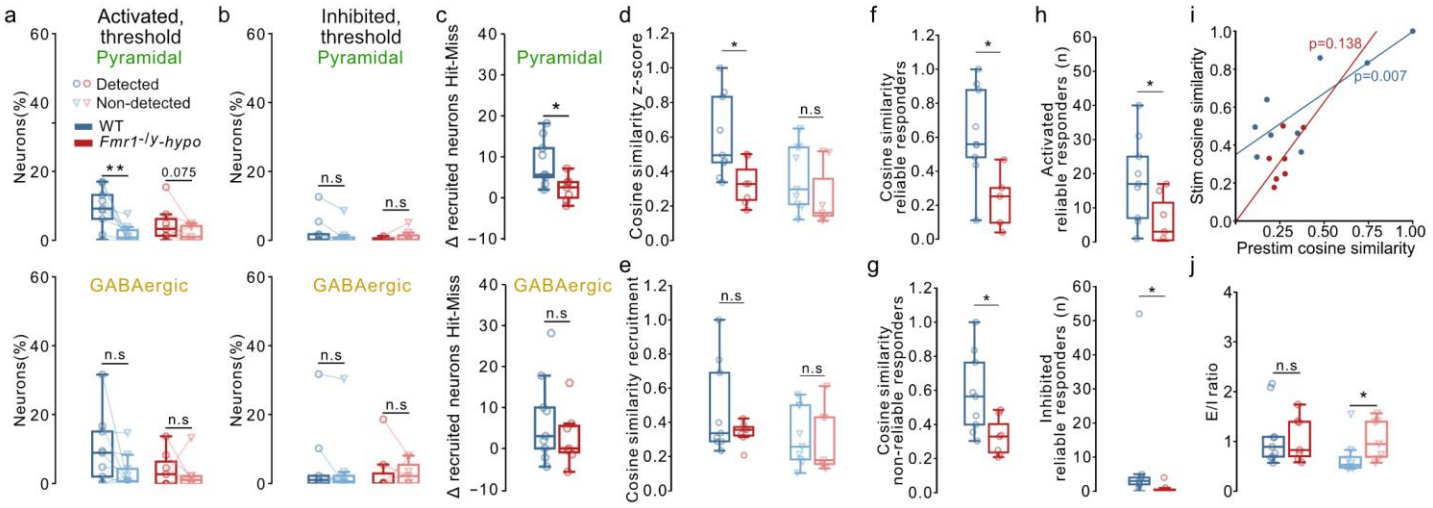

Figure 3. **Response decoding in *Fmr1*$^{-/y}$-hyposensitive mice is vulnerable to the ongoing network state**

For all panels: 1 session, ~10 repetitions of each amplitude per mouse. For all panels apart from **f, j,:** n=9 WT, 7 *Fmr1*$^{-/y}$-hyposensitive mice. For panel **f,:** n=9 WT, 5 *Fmr1*$^{-/y}$-hyposensitive mice. For panel **j,:** Detected: n=9 WT, 8 *Fmr1*$^{-/y}$-hyposensitive mice; Non-detected: n=7 WT, 7 *Fmr1*$^{-/y}$-hyposensitive mice**.** **a,** Percentage of activated pyramidal neurons (top) and GABAegic interneurons (bottom) for the threshold stimulus amplitude of each mouse during detected (dark color, circles) and non-detected trials (light color, triangles). **b,** Same as (**a,**) but for inhibited pyramidal neurons (top) and GABAegic interneurons (bottom). **c,** Δ difference in the percentage of recruited pyramidal neurons (top) and recruited GABAergic interneurons (bottom) between detected (Hit) and non-detected (Miss) trials. **d,** Cosine similarity of the average z-score responses between each pair of detected (dark color, circles) and non-detected (light color, triangles) threshold trials. **e,** Cosine similarity of the identity of recruited neurons between detected (dark color, circles) and non-detected (light color, triangles) threshold trials. **f,** Cosine similarity of the average z-score activity of reliable responders between each pair of detected threshold trials. **g,** same as **(f,)** but for non-reliable responders. **h,** Number of activated (top) and inhibited (bottom) reliable responders in detected threshold trials. **i,** Correlation of cosine similarity of the average z-score responses between each pair of detected threshold trials with the cosine similarity in the prestimulus responses of the same neurons (average z-score, 500 ms). **j,** Excitation/Inhibition (E/I) ratio calculated as number of activated pyramidal neurons divided by the number of activated GABAergic interneurons during detected (dark color, circles) and non-detected trials (light color, triangles). P values were computed using a Wilcoxon signed-rank test for panels **a, b,**; two-sided t-test for panels **c, d, e, f, g, h, j,**; Mann-Whitney test for panels **d, e, h,**; and Pearson correlation coefficient for panel **i.** **P < 0.01, *P < 0.05 or n.s, not significant.

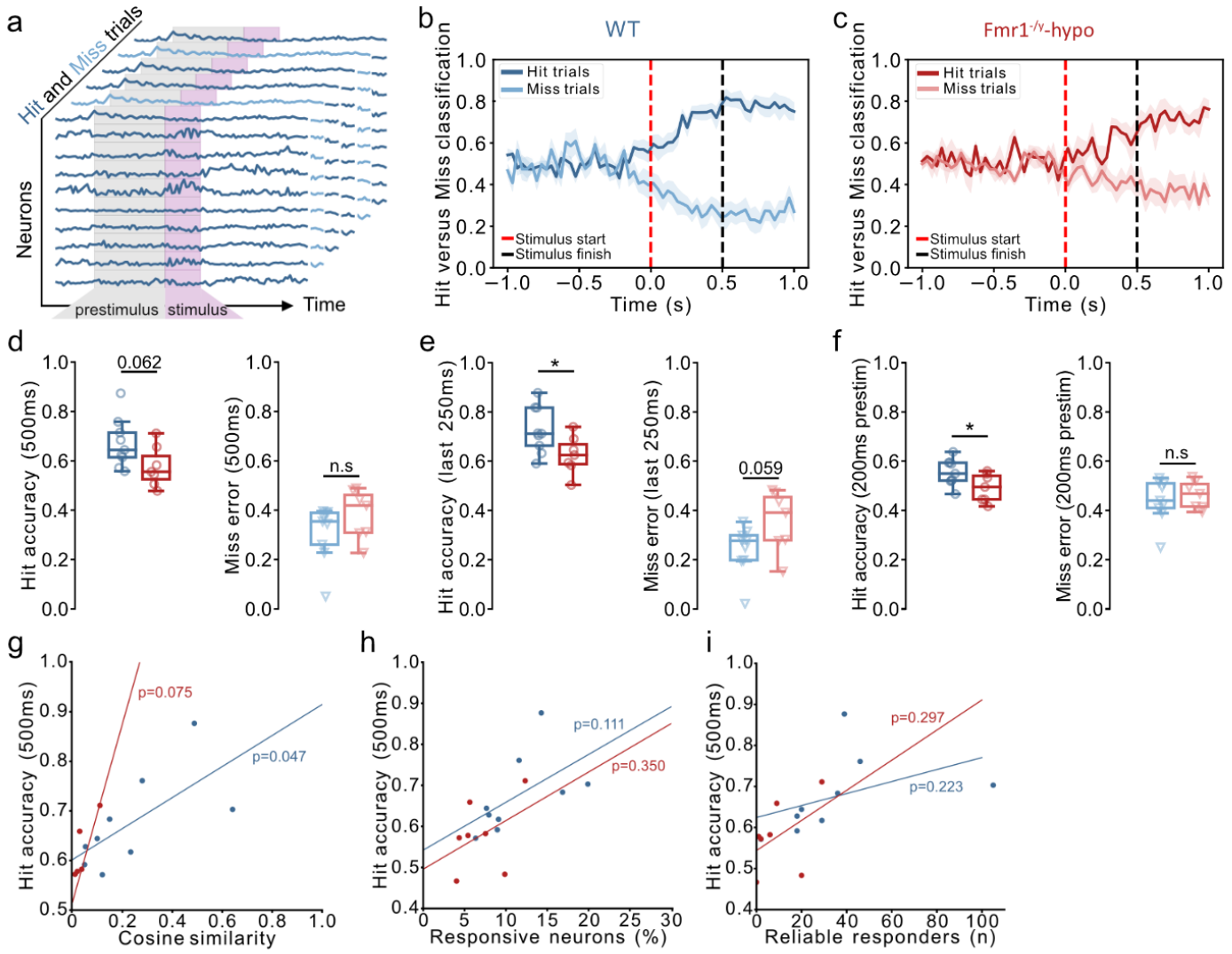

Figure 4. **Unreliable stimulus encoding impedes response decoding in *Fmr1*$^{-/y}$-hyposensitive mice**

For all panels: n=9 WT, 7 *Fmr1*$^{-/y}$-hyposensitive mice, 1 session, ~10 repetitions of each amplitude per mouse. **a,** Schema showing the training strategy of the logistic regression model, with datasets including prestimulus activity (1 s), tactile stimulation (500 ms), post-stimulus activity (500 ms). Classifiers were trained on each frame to decode if the trial was detected (Hit) or non-detected (Miss) (adapted from ref[50]). **b,** Response decoding in WT mice. Stimulus start is indicated by a red dashed line and stimulus end by a black dashed line. The dark-blue line represents true Hit classification and the light-blue line represents false Hit (Miss error) classification. **c,** Same as (**b,**) but for Fmr1$^{-/y}$-hyposensitive mice. **d,** Average Hit accuracy (left) and Miss error (right) of the classifiers on the total duration of the stimulation (500 ms). **e,** Same as (**d,**) but for the last 250 ms of stimulation. **f,** Same as (**d,**) but for the 200 ms prestimulus period before stimulus onset. **g,** Correlation of trial-by-trial similarity (cosine similarity) with the average Hit accuracy of the classifiers during stimulation (500 ms). **h,** Correlation of percentage of responsive neurons with the average Hit accuracy of the classifiers during stimulation (500 ms). **i,** Correlation of the number of reliable responders with the average Hit accuracy of the classifiers during stimulation (500 ms). P values were computed using two-sided t-test for panel **d, e, f,;** Mann-Whitney U test for panel **d, f,;** Pearson correlation coefficient for panels **g, h, i.** *P < 0.05 or n.s, not significant.

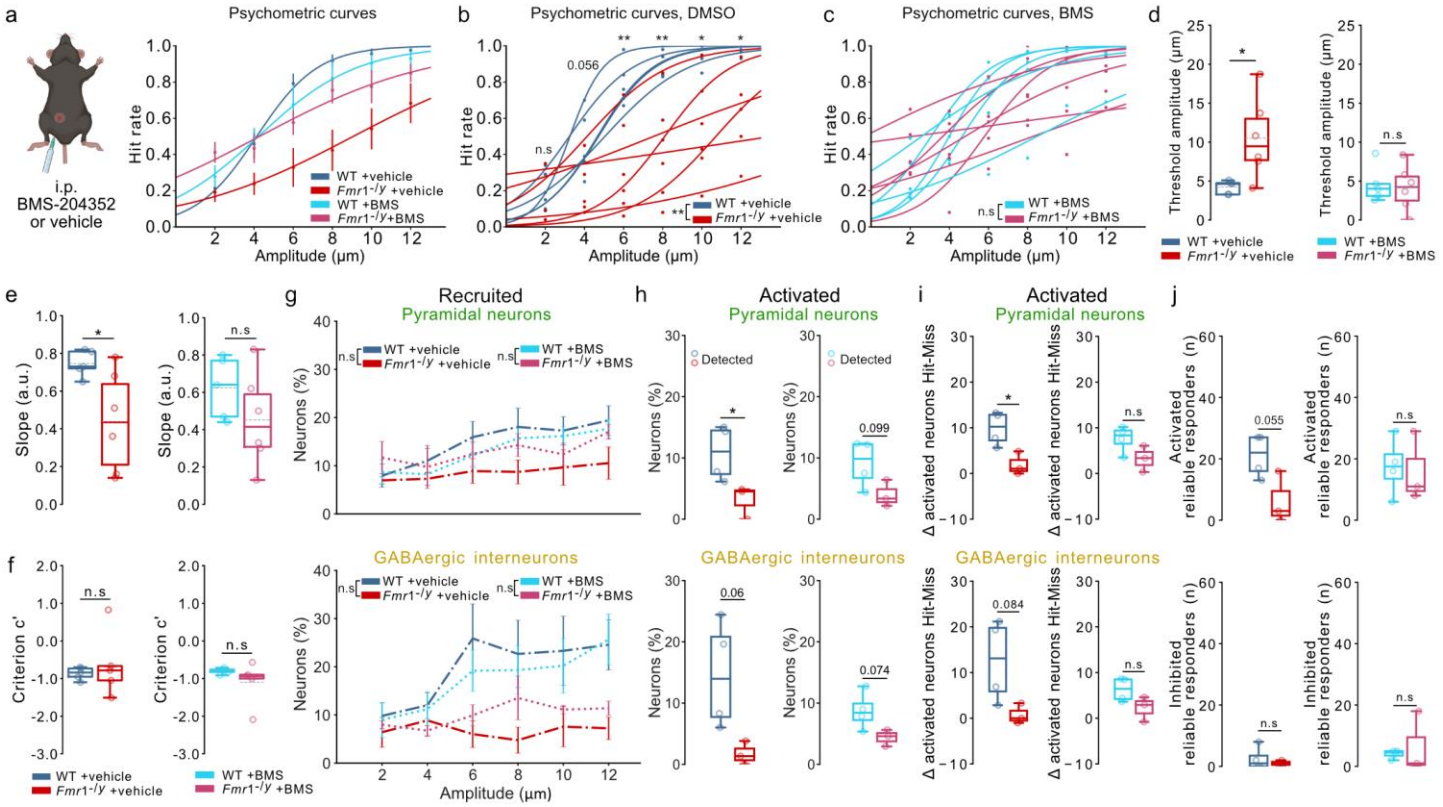

Figure 5. **BK_{CA} agonist improves tactile perception in *Fmr1*$^{-/y}$ mice by enhancing stimulus encoding in S1-FP**

For panels **a,-e,**: n=5 WT, 6 *Fmr1*$^{-/y}$ mice, ~30 repetitions of each amplitude per mouse for vehicle, ~39 repetitions for BMS. For panel **f,**: n=5 WT, 5 *Fmr1*$^{-/y}$ mice, on average ~32 repetitions of each amplitude per mouse for vehicle, ~41 repetitions for BMS. For panels **g,-j,**: n=4 WT, 3 *Fmr1*$^{-/y}$ mice,1 session with ~10 repetitions of each amplitude per mouse for vehicle and BMS. **a,** Left: Intraperitoneal injection of BMS-204352 (BMS) or vehicle. Right: Psychometric curves fitted on average Hit rates for each stimulus amplitude for WT +vehicle (blue), *Fmr1*$^{-/y}$ mice +vehicle (dark red), WT +BMS (cyan) and *Fmr1*$^{-/y}$ mice +BMS (pink). **b,** Psychometric curves of each individual mouse for WT +vehicle (blue), *Fmr1*$^{-/y}$ +vehicle mice (dark red). **c,** Psychometric curves of each individual mouse for WT +BMS (cyan), *Fmr1*$^{-/y}$ +BMS mice (pink). **d,** Detection thresholds calculated based on the psychometric curves with vehicle (left) and BMS treatment (right). **e,** Perceptual accuracy calculated based on the slope of the psychometric curves with vehicle (left) and BMS treatment (right). **f,** Relative criterion c' depicting licking strategy with vehicle (left) and BMS treatment (right). **g,** Average percentage of recruited pyramidal neurons (top) and GABAegic interneurons (bottom) for each stimulus amplitude. **h,** Percentage of activated pyramidal neurons (top) and GABAergic interneurons (bottom) in detected trials. **i,** Δ difference in the percentage of activated pyramidal neurons (top) and GABAergic interneurons (bottom) between detected (Hit) and non-detected (Miss) trials. **j,** Number of activated (top) and inhibited (bottom) reliable responders in detected threshold trials. P values were computed using an one-way ANOVA for panel **b, c,;** a mixed-ANOVA for panel **g**; and a two-sided t-test for panels **b, d, e, f, g, h, i, j**. **P < 0.01, *P < 0.05 or n.s (not significant).

References

1. American Psychiatric Association. *Diagnostic and statistical manual of mental disorders (5th ed.)*. (2013). doi:https://doi.org/10.1176/appi.books.9780890425596.

2. Balasco, L., Provenzano, G. & Bozzi, Y. Sensory Abnormalities in Autism Spectrum Disorders: A Focus on the Tactile Domain, From Genetic Mouse Models to the Clinic. *Front. Psychiatry* **10**, 1–17 (2020).

3. Foss-Feig, J. H., Heacock, J. L. & Cascio, C. J. Tactile responsiveness patterns and their association with core features in autism spectrum disorders. *Res. Autism Spectr. Disord.* **6**, 337–344 (2012).

4. Thye, M. D., Bednarz, H. M., Herringshaw, A. J., Sartin, E. B. & Kana, R. K. The impact of atypical sensory processing on social impairments in autism spectrum disorder. *Dev. Cogn. Neurosci.* **29**, 151–167 (2018).

5. Zhai, J. *et al.* Correlation and predictive ability of sensory characteristics and social interaction in children with autism spectrum disorder. *Front. Psychiatry* **14**, 1056051 (2023).

6. He, J. L. *et al.* A working taxonomy for describing the sensory differences of autism. *Mol. Autism* **14**, 15 (2023).

7. Baranek, G. T. *et al.* Hyporesponsiveness to Social and Nonsocial Sensory Stimuli in Children with Autism, Children with Developmental Delays, and Typically Developing Children. *Dev. Psychopathol.* **25**, 307 (2013).

8. Haigh, S. M., Minshew, N., Heeger, D. J., Dinstein, I. & Behrmann, M. Over-Responsiveness and Greater Variability in Roughness Perception in Autism. *Autism Res.* **9**, 393–402 (2016).

9. Cascio, C. J., Lorenzi, J. & Baranek, G. T. Self-Reported Pleasantness Ratings and Examiner-Coded Defensiveness in Response to Touch in Children with ASD: Effects of Stimulus Material and Bodily Location. *J. Autism Dev. Disord.* **46**, 1528–1537 (2016).

10. Kadlaskar, G., Seidl, A., Tager-Flusberg, H., Nelson, C. A. & Keehn, B. Atypical Response to Caregiver Touch in Infants at High Risk for Autism Spectrum Disorder. *J. Autism Dev. Disord.* **49**, 2946–2955 (2019).

11. Salkić, N., Ahmetović, Z., Velić, S., Krnojelac, L. & Nazor, V. Difficulties of the tactile sensory system sensory integration of children with autism. *Tech. Soc. Sci. J.* **27**, 502–510 (2022).

12. Puts, N. A. J., Wodka, E. L., Tommerdahl, M., Mostofsky, S. H. & Edden, R. A. E. Impaired tactile processing in children with autism spectrum disorder. *J. Neurophysiol.* **111**, 1803–1811 (2014).

13. Asaridou, M. *et al.* Could Sensory Differences Be a Sex-Indifferent Biomarker of Autism? Early Investigation Comparing Tactile Sensitivity Between Autistic Males and Females. *J.*

Autism Dev. Disord. 1–17 (2022) doi:10.1007/S10803-022-05787-6/FIGURES/6.

14. Güçlü, B., Tanidir, C., Mukaddes, N. M. & Ünal, F. Tactile sensitivity of normal and autistic children. *Somatosens. Mot. Res.* **24**, 21–33 (2007).

15. Cascio, C. *et al.* Tactile perception in adults with autism: a multidimensional psychophysical study. *J. Autism Dev. Disord.* **38**, 127–137 (2008).

16. Kim, J. H. & Kim, S. P. Neuroimaging of Tactile Information Processing. *Investig. Magn. Reson. Imaging* **27**, 1–9 (2023).

17. Marco, E. J. *et al.* Children With Autism Show Reduced Somatosensory Response: An MEG Study. *Autism Res.* **5**, 340–351 (2012).

18. Cascio, C. J., Gu, C., Schauder, K. B., Key, A. P. & Yoder, P. Somatosensory event-related potentials and association with tactile behavioral responsiveness patterns in children with ASD. *Brain Topogr.* **28**, 895 (2015).

19. Puts, N. A. J. *et al.* Reduced GABA and Altered Somatosensory Function in Children with Autism Spectrum Disorder. *Autism Res.* **10**, 608 (2017).

20. Sapey-Triomphe, L. A., Lamberton, F., Sonié, S., Mattout, J. & Schmitz, C. Tactile hypersensitivity and GABA concentration in the sensorimotor cortex of adults with autism. *Autism Res.* **12**, 562–575 (2019).

21. Coskun, M. A. *et al.* How somatic cortical maps differ in autistic and typical brains. *Neuroreport* **20**, 175–179 (2009).

22. Chen, Q. *et al.* Dysfunction of cortical GABAergic neurons leads to sensory hyper-reactivity in a Shank3 mouse model of ASD. *Nat. Neurosci.* **23**, 520–532 (2020).

23. Purves, D. *et al.* Mechanoreceptors Specialized to Receive Tactile Information. (2001).

24. Maricich, S. M., Morrison, K. M., Mathes, E. L. & Brewer, B. M. Rodents Rely on Merkel Cells for Texture Discrimination Tasks. *J. Neurosci.* **32**, 3296 (2012).

25. Abraira, V. E. & Ginty, D. D. The sensory neurons of touch. *Neuron* **79**, 618–639 (2013).

26. Sinclair, D., Oranje, B., Razak, K. A., Siegel, S. J. & Schmid, S. Sensory processing in autism spectrum disorders and Fragile X syndrome—From the clinic to animal models. *Neurosci. Biobehav. Rev.* **76**, 235 (2017).

27. Ferraguto, C., Bouleau, Y., Peineau, T., Dulon, D. & Pietropaolo, S. Hyperacusis in the Adult Fmr1-KO Mouse Model of Fragile X Syndrome: The Therapeutic Relevance of Cochlear Alterations and BKCa Channels. *Int. J. Mol. Sci.* **24**, 11863 (2023).

28. Bolton, T. A. W., Freitas, L. G. A., Jochaut, D., Giraud, A. L. & Van De Ville, D. Neural responses in autism during movie watching: Inter-individual response variability co-varies with symptomatology. *Neuroimage* **216**, 116571 (2020).

29. Scheerer, N. E. *et al.* Exploring sensory phenotypes in autism spectrum disorder. *Mol.*

Autism **12**, 1–16 (2021).

30. Guo, X. *et al.* Inter-individual heterogeneity of functional brain networks in children with autism spectrum disorder. *Mol. Autism* **13**, 1–13 (2022).

31. Vinçon-Leite, A. *et al.* Identifying interindividual variability of social perception and associated brain anatomical correlations in children with autism spectrum disorder using eye-tracking and diffusion tensor imaging MRI (DTI-MRI). *Cereb. Cortex* **34**, (2024).

32. Valiquette, V. *et al.* Examining litter specific variability in mice and its impact on neurodevelopmental studies. *Neuroimage* **269**, (2023).

33. Bechard, A., Nicholson, A. & Mason, G. Litter Size Predicts Adult Stereotypic Behavior in Female Laboratory Mice. *J. Am. Assoc. Lab. Anim. Sci.* **51**, 407 (2012).

34. Healy, K., McNally, L., Ruxton, G. D., Cooper, N. & Jackson, A. L. Metabolic rate and body size are linked with perception of temporal information. *Anim. Behav.* **86**, 685–696 (2013).

35. Dinuzzo, M. *et al.* Perception is associated with the brain's metabolic response to sensory stimulation. *Elife* **11**, (2022).

36. Giulivi, C. *et al.* Mitochondrial dysfunction in autism. *JAMA* **304**, 2389–2396 (2010).

37. Dhillon, S., A. Hellings, J. & G. Butler, M. Genetics and mitochondrial abnormalities in autism spectrum disorders: a review. *Curr. Genomics* **12**, 322–332 (2011).

38. Goh, S., Dong, Z., Zhang, Y., DiMauro, S. & Peterson, B. S. Mitochondrial dysfunction as a neurobiological subtype of autism spectrum disorder: evidence from brain imaging. *JAMA psychiatry* **71**, 665–671 (2014).

39. Barone, R. *et al.* Mitochondrial Fatty Acid β-Oxidation and Resveratrol Effect in Fibroblasts from Patients with Autism Spectrum Disorder. *J. Pers. Med.* **11**, (2021).

40. Frye, R. E. *et al.* Mitochondria May Mediate Prenatal Environmental Influences in Autism Spectrum Disorder. *J. Pers. Med.* **11**, (2021).

41. Noel, J. P., Lakshminarasimhan, K. J., Park, H. & Angelaki, D. E. Increased variability but intact integration during visual navigation in Autism Spectrum Disorder. *Proc. Natl. Acad. Sci. U. S. A.* **117**, 11158–11166 (2020).

42. Wang, Q. *et al.* Investigating intra-individual variability of face scanning in autistic children. *https://doi.org/10.1177/13623613211064373* **26**, 1752–1764 (2021).

43. Milne, E. Increased Intra-Participant Variability in Children with Autistic Spectrum Disorders: Evidence from Single-Trial Analysis of Evoked EEG. *Front. Psychol.* **2**, (2011).

44. Dinstein, I. *et al.* Unreliable Evoked Responses in Autism. *Neuron* **75**, 981–991 (2012).

45. Kovarski, K. *et al.* Reduced visual evoked potential amplitude in autism spectrum disorder, a variability effect? *Transl. Psychiatry* **9**, (2019).

46. Bouet, V. *et al.* The adhesive removal test: a sensitive method to assess sensorimotor deficits in mice. *Nat. Protoc.* **4**, 1560–1565 (2009).

47. Green, D., & Swets, J. *Signal detection theory and psychophysics*. (John Wiley, 1966).

48. Gescheider, G. A. *Psychophysics (3rd ed.). Psychology Press* (1997).

49. Bhaskaran, A. A. *et al.* Endogenous noise of neocortical neurons correlates with atypical sensory response variability in the Fmr1−/y mouse model of autism. *Nat. Commun. 2023 141* **14**, 1–16 (2023).

50. Rowland, J. M. *et al.* Propagation of activity through the cortical hierarchy and perception are determined by neural variability. *Nat. Neurosci.* **26**, 1584–1594 (2023).

51. Rubenstein, J. L. R. & Merzenich, M. M. Model of autism: Increased ratio of excitation/inhibition in key neural systems. *Genes, Brain Behav.* **2**, 255–267 (2003).

52. Sohal, V. S. & Rubenstein, J. L. R. Excitation-inhibition balance as a framework for investigating mechanisms in neuropsychiatric disorders. doi:10.1038/s41380-019-0426-0.

53. Tavassoli, T. *et al.* Altered tactile processing in children with autism spectrum disorder. *Autism Res.* **9**, 616–620 (2016).

54. Pereira, M. *et al.* Evidence accumulation relates to perceptual consciousness and monitoring. *Nat. Commun. 2021 121* **12**, 1–11 (2021).

55. Laumonnier, F. *et al.* Association of a functional deficit of the BKCa channel, a synaptic regulator of neuronal excitability, with autism and mental retardation. *Am. J. Psychiatry* **163**, 1622–1629 (2006).

56. Deng, P. Y. *et al.* FMRP Regulates Neurotransmitter Release and Synaptic Information Transmission by Modulating Action Potential Duration via BK channels. *Neuron* **77**, 696 (2013).

57. Guglielmi, L. *et al.* Update on the implication of potassium channels in autism: K(+) channelautism spectrum disorder. *Front. Cell. Neurosci.* **9**, (2015).

58. Zhang, Y. *et al.* Dendritic channelopathies contribute to neocortical and sensory hyperexcitability in Fmr1-/y mice. *Nat. Neurosci.* **17**, 1701–1709 (2014).

59. Carreno-Munoz, M. I. *et al.* Potential Involvement of Impaired BKCa Channel Function in Sensory Defensiveness and Some Behavioral Disturbances Induced by Unfamiliar Environment in a Mouse Model of Fragile X Syndrome. *Neuropsychopharmacology* **43**, 492–502 (2018).

60. Scott, K. E. *et al.* Closing the species gap: Translational approaches to studying sensory processing differences relevant for autism spectrum disorder. *Autism Res.* **14**, 1322–1331 (2021).

61. Tillmann, J. *et al.* Dissecting the phenotypic heterogeneity in sensory features in autism spectrum disorder: A factor mixture modelling approach. *Mol. Autism* **11**, 1–15 (2020).

62. Scheerer, N. E. *et al.* Exploring sensory phenotypes in autism spectrum disorder. *Mol. Autism* **12**, 1–16 (2021).

63. Orefice, L. L. L. *et al.* Peripheral Mechanosensory Neuron Dysfunction Underlies Tactile and Behavioral Deficits in Mouse Models of ASDs. *Cell* **166**, 299–313 (2016).

64. Orefice, L. L. *et al.* Targeting Peripheral Somatosensory Neurons to Improve Tactile-Related Phenotypes in ASD Models. *Cell* **178**, 867-886.e24 (2019).

65. Deemyad, T. *et al.* Lateralized Decrease of Parvalbumin+ Cells in the Somatosensory Cortex of ASD Models Is Correlated with Unilateral Tactile Hypersensitivity. *Cereb. Cortex* **32**, 554–568 (2022).

66. He, C. X. *et al.* Tactile defensiveness and impaired adaptation of neuronal activity in the Fmr1 knock-out mouse model of autism. *J. Neurosci.* **37**, 6475–6487 (2017).

67. Haznedar, M. M. *et al.* Limbic circuitry in patients with autism spectrum disorders studied with positron emission tomography and magnetic resonance imaging. *Am. J. Psychiatry* **157**, 1994–2001 (2000).

68. Lumaban, J. G. & Nelson, D. L. The Fragile X proteins Fmrp and Fxr2p cooperate to regulate glucose metabolism in mice. *Hum. Mol. Genet.* **24**, 2175 (2015).

69. Licznerski, P. *et al.* ATP Synthase c-Subunit Leak Causes Aberrant Cellular Metabolism in Fragile X Syndrome. *Cell* **182**, 1170-1185.e9 (2020).

70. Cohen, L. G., Bandinelli, S., Sato, S., Kufta, C. & Hallett, M. Attenuation in detection of somatosensory stimuli by transcranial magnetic stimulation. *Electroencephalogr. Clin. Neurophysiol.* **81**, 366–376 (1991).

71. McKay, D. R., Ridding, M. C. & Miles, T. S. Magnetic stimulation of motor and somatosensory cortices suppresses perception of ulnar nerve stimuli. *Int. J. Psychophysiol.* **48**, 25–33 (2003).

72. Tamè, L. & Holmes, N. P. Involvement of human primary somatosensory cortex in vibrotactile detection depends on task demand. *Neuroimage* **138**, 184–196 (2016).

73. Pérez-Ortega, J., Akrouh, A. & Yuste, R. Stimulus encoding by specific inactivation of cortical neurons. *Nat. Commun. 2024 151* **15**, 1–14 (2024).

74. Dalgleish, H. W. P. *et al.* How many neurons are sufficient for perception of cortical activity? *Elife* **9**, 1–99 (2020).

75. Park, W. J., Schauder, K. B., Zhang, R., Bennetto, L. & Tadin, D. High internal noise and poor external noise filtering characterize perception in autism spectrum disorder. *Sci. Rep.* **7**, (2017).

76. Yang, H., Kwon, S. E., Severson, K. S. & O'Connor, D. H. Origins of choice-related activity in mouse somatosensory cortex. *Nat. Neurosci.* **19**, 127 (2016).

77. Finkel, E. A. *et al.* Tactile processing in mouse cortex depends on actioncontext. *Cell Rep.*

43, 113991 (2024).

78. Antoine, M. W., Langberg, T., Schnepel, P. & Feldman, D. E. Increased Excitation-Inhibition Ratio Stabilizes Synapse and Circuit Excitability in Four Autism Mouse Models. *Neuron* **101**, 648-661.e4 (2019).

79. Michaelson, S. D. *et al.* SYNGAP1 heterozygosity disrupts sensory processing by reducing touch-related activity within somatosensory cortex circuits. *Nat. Neurosci.* **21**, (2018).

80. Contractor, A., Klyachko, V. A. & Portera-Cailliau, C. Altered neuronal and circuit excitability in Fragile X Syndrome. *Neuron* **87**, 699 (2015).

81. Carandini, M. & Heeger, D. J. Normalization as a canonical neural computation. *Nat. Rev. Neurosci.* **13**, 51 (2012).

82. Milne, E. Increased intra-participant variability in children with autistic spectrum disorders: Evidence from single-trial analysis of evoked EEG. *Front. Psychol.* **2**, 1–12 (2011).

83. Haigh, S. M., Heeger, D. J., Dinstein, I., Minshew, N. & Behrmann, M. Cortical variability in the sensory-evoked response in autism. *J. Autism Dev. Disord.* **45**, 1176 (2015).

84. Hébert, B. *et al.* Rescue of fragile X syndrome phenotypes in Fmr1 KO mice by a BKCa channel opener molecule. *Orphanet J. Rare Dis.* **9**, (2014).

85. Silverman, J. L. *et al.* GABAB Receptor Agonist R-Baclofen Reverses Social Deficits and Reduces Repetitive Behavior in Two Mouse Models of Autism. *Neuropsychopharmacology* **40**, 2228–2239 (2015).

86. Möhrle, D., Wang, W., Whitehead, S. N. & Schmid, S. GABAB Receptor Agonist R-Baclofen Reverses Altered Auditory Reactivity and Filtering in the Cntnap2 Knock-Out Rat. *Front. Integr. Neurosci.* **15**, 1–27 (2021).

87. Huang, Q. *et al.* GABA B receptor modulation of visual sensory processing in adults with and without autism spectrum disorder. *Sci. Transl. Med.* **14**, 7859 (2022).

88. Lane, A. E., Molloy, C. A. & Bishop, S. L. Classification of Children With Autism Spectrum Disorder by Sensory Subtype: A Case for Sensory-Based Phenotypes. *Autism Res.* **7**, 322–333 (2014).

89. Lyons-Warren, A. M., Wangler, M. F. & Wan, Y.-W. Cluster Analysis of Short Sensory Profile Data Reveals Sensory-Based Subgroups in Autism Spectrum Disorder. *Int. J. Mol. Sci.* **23**, 13030 (2022).

90. Frye, R. E., Rose, S., Boles, R. G. & Rossignol, D. A. A Personalized Approach to Evaluating and Treating Autism Spectrum Disorder. *J. Pers. Med.* **12**, (2022).

91. Harrison, L. A., Kats, A., Williams, M. E. & Aziz-Zadeh, L. The Importance of Sensory Processing in Mental Health: A Proposed Addition to the Research Domain Criteria (RDoC) and Suggestions for RDoC 2.0. *Front. Psychol.* **10**, (2019).

92. Prsa, M., Morandell, K., Cuenu, G. & Huber, D. Feature-selective encoding of substrate vibrations in the forelimb somatosensory cortex. *Nature* **567**, 384–388 (2019).

93. Hautus, M.J., Macmillan, N.A., & Creelman, C. D. *Detection Theory: A User's Guide*. (Routledge, 2021).

Acknowledgments

We would like to thank the animal housing and genotyping facilities of INSERM U1215 Neurocenter Magendie. We thank Apolline Joliot for assisting in immunohistochemistry experiments. We thank Dr. James Poulet (Max-Delbrück-Centrum für Molekulare Medizin, Berlin) for providing the capacitive sensors for the behavioral task. We thank Dr. Naoya Takahashi (Interdisciplinary Institute for Neuroscience, Bordeaux) and Dr. James Poulet (Max-Delbrück-Centrum für Molekulare Medizin, Berlin) for providing feedback on the manuscript. This project was funded by the Foundation for Medical Research Postdoc Fellowship (O.S.), INSERM (A.F.), Marcel Dassault-Fondation FondaMental Award 2019 (A.F.), Simons Foundation Autism Research Initiative (A.F.), GIS Autisme & TND (O.S.), Fondation FondaMental.

Author Information

Authors and Affiliations
INSERM, U1215 Neurocentre Magendie, 33077, Bordeaux, France
Semelidou Ourania, Théo Gauvrit, Célien Vandromme, Alexandre Cornier, Anna Saint-Jean, Yves Le Feuvre, Melanie Ginger, Andreas Frick
University of Bordeaux, 33000, Bordeaux, France
Semelidou Ourania, Théo Gauvrit, Célien Vandromme, Alexandre Cornier, Anna Saint-Jean, Yves Le Feuvre, Melanie Ginger, Andreas Frick
University of Lille, 59000 , Lille, France
Célien Vandromme

Contributions

A.F., M.G., and O.S. conceived the project and designed the experiments. O.S. performed the experiments. A.S.J. and Y.L.F. contributed to the tape removal experiments and their analysis. A.C. wrote the Python code for the behavioral experiments. O.S., T.G., and C.V. analyzed the data and wrote the necessary Python scripts. O.S. prepared the figures. O.S., T.G., and A.F. interpreted the data. O.S. wrote the manuscript, and A.F., M.G., Y.L.F., and T.G. provided feedback.

Corresponding author

Correspondence to Andreas Frick and Ourania Semelidou.

Ethics declarations

Competing interests

The authors declare no competing interests.

Inclusion and diversity statement

We support inclusive, diverse, and equitable conduct of research. We tried to use inclusive language as much as possible.